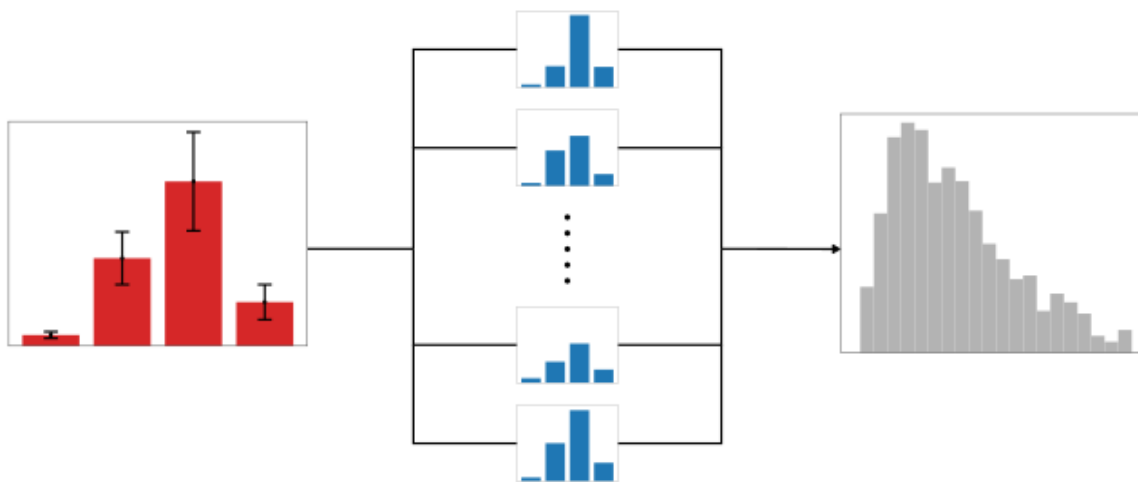




REFLECT DELIVERABLE D4.3

D4.3 IMPACT OF GEOCHEMICAL UNCERTAINTIES ON FLUID PRODUCTION AND SCALING PREDICTION



Summary:

This deliverable summarizes the methodology to estimate the impact of hydrodynamics and fluid composition uncertainties on the scaling precipitation in geothermal fields.

Authors:

Jonah Poort, TNO, Research scientist
Hidde de Zwart, TNO, Research scientist
Laura Wasch, TNO, Senior scientist
Pejman Shoeibi Omrani, TNO, Senior scientist



Title:	D4.3 Impact of geochemical uncertainties on fluid production and scaling prediction
Lead beneficiary:	TNO
Other beneficiaries:	BRGM
Due date:	30 April 2022
Nature:	Report
Diffusion:	Public
Status:	Final
Document code:	REFLECT_D4.3
DOI:	10.48440/gfz.4.8.2022.001
License information:	CC-BY-4.0
Recommended citation:	Poort, J., de Zwart, H., Wasch, L., Shoeibi Omrani, P.: <i>The H2020 REFLECT project: Deliverable 4.3 Impact of geochemical uncertainties on fluid production and scaling prediction</i> , GFZ German Research Centre for Geosciences, DOI: 10.48440/gfz.4.8.2022.001

Revision history	Author	Delivery date	Summary of changes and comments
Version 01	Poort et al.	15.03.2022	Draft version
Version 02	Shoeibi Omrani et al.	29.04.2022	Including the comments from reviewers and the results of the heat transfer reduction
Final version	Poort et al.	11.05.2022	Including the comments from external reviewers

Approval status				
	Name	Function	Date	Signature
Deliverable responsible	Pejman Shoeibi Omrani	Senior Scientist (TNO)	29/04/2022	
WP leader	Laurent Andre	Hydrogeochemist (BRGM)	25/04/2022	
Reviewer	Aris Twerda	Senior scientist (TNO)	12/04/2022	
Reviewer	Laurent Andre	Hydrogeochemist (BRGM)	25/04/2022	
Project Coordinator	Simona Regenspurg	Geochemist	4.5.2022	

This document reflects only the author's view and the European Commission is not responsible for any use that may be made of the information it contains.

TABLE OF CONTENTS

Table of contents.....	3
Figures.....	4
Tables.....	5
1 EXECUTIVE SUMMARY.....	6
2 Introduction.....	7
3 State-of-the-art.....	9
4 Methodology.....	12
4.1 Simulators.....	12
4.2 Coupled modelling Workflow.....	12
4.3 Flow-precipitation interaction.....	13
4.4 Uncertainty quantification.....	17
4.4.1 Types of uncertainty.....	17
4.4.2 Uncertainty quantification approach.....	18
4.4.3 Sobol sensitivities.....	19
4.5 Case studies.....	20
4.5.1 Case A: barite scaling modelling.....	20
4.5.2 Case B: uncertainty quantification of scaling potentials.....	20
4.5.3 Case C: modelling the impact of hydrodynamics on scaling precipitation.....	20
4.5.4 Case D: uncertainty quantification of scaling precipitation, roughness, and flow.....	20
5 Results.....	21
5.1 Results case A: Barite scaling model.....	21
5.1.1 Model set-up and initialization.....	21
5.1.2 Barite scaling potential.....	22
5.1.3 Effect strontium on barite scaling potential.....	24
5.1.4 Effect calcium and magnesium on barite scaling potential.....	25
5.2 Results case B: Impact of uncertainties on scaling potential.....	27
5.2.1 Brine composition and uncertainty bounds.....	27
5.2.2 Uncertainty in barite scaling potentials.....	28
5.2.3 Sobol sensitivities of barite scaling potential.....	32
5.3 Results case c: Impact of hydrodynamics on scaling.....	33
5.3.1 Deposition profile.....	33
5.3.2 Flow velocity profile and average flowrate.....	34
5.3.3 Heat flux through pipe wall.....	36
5.4 Results case D: Impact of uncertainties on scaling.....	40
5.4.1 Uncertainty in deposition layer height.....	40
5.4.2 Uncertainty in flowrates.....	41
6 CONCLUSION & recommendations.....	42
6.1 Conclusions.....	42
6.1.1 Scaling model.....	42
6.1.2 Impact of uncertainties on scaling.....	43
6.1.3 Impact of hydrodynamics on scaling.....	43
6.2 Recommendations.....	44
6.2.1 Scaling model.....	44

6.2.2	Impact of hydrodynamics on scaling.....	44
6.2.3	Impact of uncertainties on scaling.....	44
7	References.....	45

FIGURES

Figure 1.	Schematic of combining three modelling elements within a multiphase flow solver, the figures of the transport and deposition mechanisms are by (Schutte, 2016).....	8
Figure 2.	SEM image of barite crystals under laminar flow conditions (Re = 176, left) and turbulent flow conditions (Re = 11249, right). Image from (Yan, et al., 2016).....	11
Figure 3.	Workflow of the coupled flow-chemistry modelling framework. Image adapted from (Twerda & Veltin, 2014).....	13
Figure 4.	Illustrated view of the deposition profile of single grid cell.....	14
Figure 5.	Force diagram of one layer of scales.....	15
Figure 6.	Illustration of the deposition layer, after one and two time step(s).....	17
Figure 7.	Graphical depiction of the uncertainty quantification approach.....	18
Figure 8.	Example of samples generated using a (pseudo-)random uniform distribution (left) and a Sobol sampling strategy. Points in red correspond to the first 10 samples, those in blue to the first 100 samples, and green the remaining samples. As can be seen, the Sobol samples are distributed more evenly throughout the sampling box.....	19
Figure 9.	Barite precipitation simulated for cooling from 100 to 20 °C.....	23
Figure 10.	Kinetic barite precipitation at fixed conditions of 30 °C and 10 bar, simulated for a time span of 5 years.....	23
Figure 11.	Kinetic barite precipitation at fixed conditions of 30 °C and 10 bar, simulated for a time span of 10 minutes.....	24
Figure 12.	Barite saturation index (SI) simulated for cooling from 100 to 20 °C.....	24
Figure 13.	Precipitation of a barite-celestite solid solution, simulated for cooling from 105 to 30 °C.....	25
Figure 14.	The effect of different initial calcium concentrations in mg/kg-water on barite precipitation, simulated for cooling from 100 to 20 °C.....	26
Figure 15.	The effect of different initial magnesium concentrations in mg/kg-water on barite precipitation, simulated for cooling from 100 to 20 °C.....	26
Figure 16.	Uncertainties in the fluid composition measurements (in mg/L) for a group of wells in a formation (top) and a single doublet in the same formation (bottom), the solid line indicates the mean value and the dashed lines are the standard deviation.....	27
Figure 17.	Barite scaling amounts calculated using PHREEQC at 70 °C and 10 bar for the smaller well variations (left), and larger formation variations (right). Results are plotted both as a box plots (top) and histogram plots (bottom). The black dashed lines indicate the mean value of barite scaling distribution, red lines dashed lines are one standard deviation away from the mean, and the purple dash-dotted lines indicate the barite scaling amount corresponding to the nominal brine composition.....	29
Figure 18.	Barite scaling amount distributions at five different temperature-pressure combinations (from top to bottom, left to right: 100 °C, 10 bar; 90 °C, 8.75 bar; 70 °C, 7.5 bar; 50 °C, 6.25 bar; and 40 °C, 5 bar). The black dashed lines indicate the mean value of barite	

scaling distribution and the purple dash-dotted lines indicate the barite scaling amount corresponding to the nominal brine composition.....31

Figure 19 First and total order Sobol sensitivities (top) as well as second order sensitivities (bottom) for the eight elements included in the brine uncertainty quantification for the smaller well variations (left) and larger formation variations (right).....33

Figure 20. Shear stress as a function of critical cone height (left) and deposition profile of barite over time (right).....34

Figure 21. Flow velocity over time.....35

Figure 22. Average volumetric flowrate over time.....35

Figure 23: Thermal resistance comparison between conductive and convective heat transfer.38

Figure 24: Relative changes in heat flux in heat exchanger (relative to the initial heat flux without any precipitation).....38

Figure 25: Relative average heat transfer in heat exchanger.....39

Figure 26: Influence of deposition profile in heat exchanger on barite precipitation.....39

Figure 27. Deposition height uncertainty of barite precipitation.....40

Figure 28. Uncertainty in averaged volumetric flowrate.....41

TABLES

Table 1: Mechanical properties of barite. Data from (Wen, et al., 2020) 11

Table 2 Gas composition of the case study fluid.....22

Table 3 Brine composition of the case study fluid.....22

Table 4. Nominal concentrations and minimum and maximum percentual deviations of elements included in the brine uncertainty quantification analysis.....28

1 EXECUTIVE SUMMARY

This deliverable summarizes the activities related to the development of predictive models to simulate the impact of fluid flow hydrodynamics and chemical composition uncertainties on the production behavior of geothermal assets. Specifically, in this report, the mineral precipitation behavior of the geothermal fluid was studied as both uncertainties in the fluid composition and the interaction between the fluid flow hydrodynamics and mineral precipitation can impact the deposition of the scaling.

A workflow was developed to couple a multiphase flow solver to thermodynamics libraries and models which are used to simulate the precipitation amount and kinetics of different geothermal minerals. This coupled workflow will enable a better estimation of the location and amount of precipitated minerals in different location of a geothermal system. A detailed roughness model was developed to simulate the impact of mineral deposition to the fluid flow. In addition, an uncertainty quantification workflow was combined with the modelling framework to estimate the uncertainty bounds of the scaling and precipitation resulted from uncertainties in the fluid composition characterization and operational settings.

The modelling and uncertainty quantification workflow was demonstrated on a barite precipitation case study in a heat exchanger. Initially, the impact of geo-chemical uncertainties (in fluid composition) on the mineral precipitation was assessed. Afterwards, the coupled fluid flow and precipitation model with the developed roughness model was tested. Finally, the coupled uncertainty quantification workflow with the coupled model was simulated to assess the impact of fluid composition uncertainties on mineral deposition. As an outcome of the simulation, the impact of uncertainties in the mineral deposition on reduction in the production rate and heat transfer (within the heat exchanger) was calculated.

The developed framework is flexible and generic which can be applied to various production and operational challenges in geothermal assets. In the future, the workflow can be used to optimize the design and operation of geothermal assets considering various sources of uncertainties which is not only fluid composition but also operational conditions (link to D4.5 REFLECT), robust modelling of other geo-chemical and flow assurance challenges in geothermal sites or even developing geo-chemical risk maps for different sites within EU (link to WP3 REFLECT).

2 INTRODUCTION

Mineral scaling is one of the main challenges complicating the efficient operation of geothermal systems. The deposition of solid scales can lead to clogging of wells, reservoirs or surface facilities, reduction of flowrates within the wellbore and topside equipment, and impede the transfer of heat within heat exchanger systems, ultimately affecting the lifespan and economic viability of geothermal systems. Based on the chemical composition of the geothermal brine, which depends on the geological formation and on the operational settings, different types and amounts of scales can form within the system. Examples include calcite (CaCO_3), barite (BaSO_4), celestite (SrSO_4), as well as lead-based and silica scales (which are mainly observed in high-enthalpy systems) (Regenspurg, et al., 2014). In addition, the thermo- and hydrodynamics of the system, i.e., the flowrates, pressures and temperatures, will largely determine the precise location and severity of scaling.

Through specifying the topside pressure, heat extraction, and other parameters, these latter properties can, to a certain extent, be controlled by the operator of the system. For this, having an accurate and predictive model of the system is of critical importance, as it allows for evaluating the effects of different operating conditions on the scaling potential and flow conditions in the system without having to experiment with the physical system itself.

An accurate prediction of the scaling amount and location in the geothermal systems depends heavily on (1) characterization of the geothermal fluid which is impacted by the uncertainties in the fluid sampling and analysis and (2) interaction between flow hydrodynamics and precipitation. Analysis of the impact of geochemical uncertainties and flow properties on the scaling prediction of geothermal brine would enable operators to make a better decision about the operational settings and mitigation measures.

The objective of this work was to develop an accurate and robust prediction workflow for geothermal fluid production by considering the uncertainties in the physico-chemical properties of geothermal fluids. In this work, a modelling workflow has been developed, Figure 1, that combines a flow solver which calculates the hydrodynamic properties (such as flow rate, shear stresses, ...), pressures, and temperatures in the fluid flow system with a geochemical speciation tool that calculates the scaling potentials of selected minerals (PHREEQC (Parkhurst & Appelo, 2013)) and the fluid properties, which often derives from characterization tests. The developed workflow includes the two-way coupling between scale deposits and flow properties, i.e., the fact that minerals which precipitate on equipment walls in turn affect the flowrates in the system (through changing wall diameter and roughness) as well as temperatures (through reducing heat transfer) and pressures.

However, while it is possible to manage a system's operating conditions within certain boundaries, the composition of the geothermal brine cannot be controlled as easily. Moreover, having full certainty of the brine composition is highly unlikely in the first place. Measurements contain errors, and sampling of the brine is complex and expensive, making frequent monitoring of its composition practically infeasible. As a result, the exact composition of the geothermal brine is a large source of uncertainty within the modelling workflow.

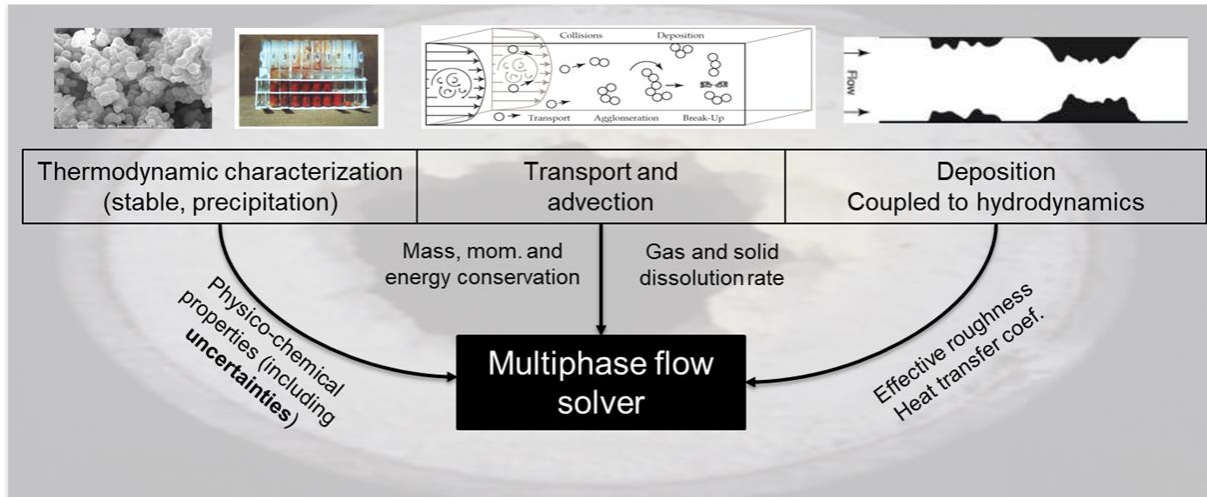


Figure 1. Schematic of combining three modelling elements within a multiphase flow solver, the figures of the transport and deposition mechanisms are by (Schutte, 2016)

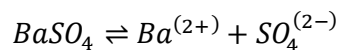
Therefore, in addition to the development of a two-way coupled modelling approach, this task also includes an additional uncertainty quantification workflow which can be integrated into the geochemical-hydrodynamic models. In this workflow, the impact of fluid composition uncertainties based on the measurements error bounds on the scaling potential, amount and resulting production behavior can be quantified. Such a workflow can be used to optimize operating conditions that mitigate the negative effects of scaling while maintaining cost-effective operation.

The models developed in this work were applied to a model brine composition from a low-enthalpy geothermal doublet which has the tendency to barite and celestite precipitation. Therefore, this work focuses primarily on the modelling of barite scales. In addition, as barite scaling is primarily dependent on temperature, all methods have initially been applied to a heat exchanger system. However, the generality of the developed workflow will allow it to be easily applied to other parts of a geothermal system, or the system in its entirety. Furthermore, depending on the nature of the minerals scaling chemistry, the models can be extended to include additional types of scales.

Note that there is no conclusive evidence that these Dutch doublets experience barite scaling even though the models indicate supersaturation. In the PERFORM-D1.3 report (Kristensen, et al., 2020), many geothermal waters were assessed for barite scaling and the vast majority of formation waters were at, or close to, equilibrium with barite at reservoir conditions and supersaturated at the surface after cooling. Despite this, significant precipitation of barite is only reported at few sites (e.g. Groß Schönebeck). This discrepancy could be related to kinetic or nucleation related retardation of precipitation, insufficient supersaturation or model inaccuracies in for example in the thermodynamic database. Although not proven for Dutch doublets, barite scaling is a common issue for geothermal systems worldwide and therefore of interest as a case study for the workflow development.

3 STATE-OF-THE-ART

In a geothermal system, brine is transported from aquifers – subsurface water reservoirs – to the surface, with the aim of extracting the thermal energy of the brine. The geothermal brine consists of several dissolved compounds – hydrocarbons, sulphates, metal ions - and gases, with unique concentrations for every aquifer. In the reservoir, the minerals and gases are approaching equilibrium with the formation water over time. Element concentrations are often enriched in saline water and can form scales due to mineral oversaturation or electrochemical reaction with the steel casing (Schreiber, et al., 2016). Barite or other sulphate scales occur in geothermal installations because the equilibrium as exists in the reservoir is disturbed by transport to the surface conditions. When changes in temperature and pressure cause the solubility to decrease, the mineral becomes oversaturated and precipitates. The solubility of barite decreases with decreasing temperature or pressure and increases with higher salinity (Zhen Wu, 2016). Barite solubility decreases with increasing pH (over pH 9), but the pH dependency is negligible between a pH of 2 and 6.5 (Zhen Wu, 2016), which is the pH relevant for Dutch siliciclastic reservoirs. The increase in barite solubility with higher salinities is due to the formation of different barium complexes which leads to the relatively high barium concentrations in formation water (the “salting in” effect, (Blount, 1977)).



Two types of mineral precipitation exist in geothermal systems (Andritsos, et al., 2002):

- **Heterogeneous precipitation:** the formation of nuclei on a surface, typically a solid-liquid interface. The interface concerned in this report is the solid-liquid interface, as the Gibbs energy of formation of a gas-liquid interface is orders of magnitude larger compared to the solid-liquid interface (Abyzov & Schmelzer, 2014). Most minerals, such as calcite, barite, celestite e.g., follow this path of precipitation, as the nucleation barrier is much lower for heterogeneous nucleation as it is for homogeneous nucleation. This type of precipitation is considered in this report.
- **Homogeneous precipitation:** the formation of nuclei inside the bulk flow. This type of precipitation does not require an interface or impurity, but the nucleation barrier is much higher. Silica tends to precipitate in this manner.

Heterogeneous precipitation will thus nucleate and grow on the pipe wall, resulting in a change in surface roughness and a decrease in effective flow area. Both parameters affect the flow profile of the brine, and they lead to a decrease in heat transfer in the heat exchanger. These phenomena impact the (local) thermo- and hydrodynamic properties, as pressure drop will increase, and less thermal energy can be extracted. This, in turn, results in a shift of precipitation quantity and location. Therefore, a two-way coupling exists between precipitation and flow hydrodynamics.

It is not straightforward to obtain an exact solution for each geothermal doublet: as the vast part of a doublet is located subsurface, measuring its brine properties induces errors. Therefore,

aleatoric uncertainties of brine composition and precipitation properties and mechanisms are also evaluated. Its magnitudes are expressed as a deviation error from the 'original' solution.

The cooled and depressurized brine flowing through a geothermal doublet is prone to scaling. Minerals tend to precipitate out of the brine when its saturation index exceed a threshold. The saturation ratio is given by the ion activity product divided by the solubility product (Sorbie & Scott Boak, 2012): $\Omega_{SR} = \frac{I_{ap}}{K_{sp}}$.

- **For $\Omega_{SR} < 1$:** The brine is undersaturated with respect to the ion, which means that those ions will stay dissolved in the brine.
- **For $\Omega_{SR} = 1$:** The brine is (critically) saturated. Ions will not precipitate, but a slight increase in ion activity or decrease in solubility product will shift the equilibrium.
- **For $\Omega_{SR} > 1$:** The brine is supersaturated, and the respective ions will react and precipitate out of the brine.

Thermodynamic models calculate chemical equilibria by using the saturation index, which is linked to the saturation ratio by the relation: $\Omega_{SI} = \log_{10}[\Omega_{SR}]$. As $\log_{10}[1] = 0$, the threshold of mineral precipitation is shifted to 0 when the saturation index is concerned.

The ion activity is the multiplicative of the molar concentration of said ion and its activity coefficient (Wright, 2007). Different models exist to calculate the activity coefficient. In this approach, the extended Debye-Hückel theory is used, due to the high salinity of geothermal brine and therefore its high ionic strength (Boersma, et al., 2018). The activity coefficient and the solubility product are both thermodynamic properties, and functions of temperature and pressure (Lei, et al., 2020). These properties are flow-dependent, thus mineral precipitation is affected by the transportation of the brine.

The heterogeneous precipitation of minerals tends to attach and deposit on the pipe walls, forming a precipitation layer. This layer reduces the effective flow area and induces a unique surface roughness. Both these phenomena impact the flow hydrodynamics. Therefore, a two-way coupling is present between mineral precipitation and hydrodynamics. In an earlier work by (Wasch, et al., 2019) a coupling between the flow properties and precipitation amount was performed, however the coupling of the impact of precipitation on the fluid properties were not considered.

To quantify the development of mineral deposition, mineral precipitation mechanics need to be analyzed: where and how do they deposit? In this report, barite precipitation is considered. Each mineral has a specific crystal structure, which is the 'preferred' stacking of atoms. Precipitated minerals in a geothermal system tend to form in their preferred shape. However, turbulent shear forces break down the crystal structure. (Yan, et al., 2016) showed that barite maintains its crystalline structure in laminar flow conditions but breaks down to conical structures under turbulent conditions. (Chen, et al., 2017) used spectrum analysis to indicate a preference of barite precipitation at a contact angle of 38 degrees in turbulent conditions. A SEM image of barite precipitation is given in Figure 2.

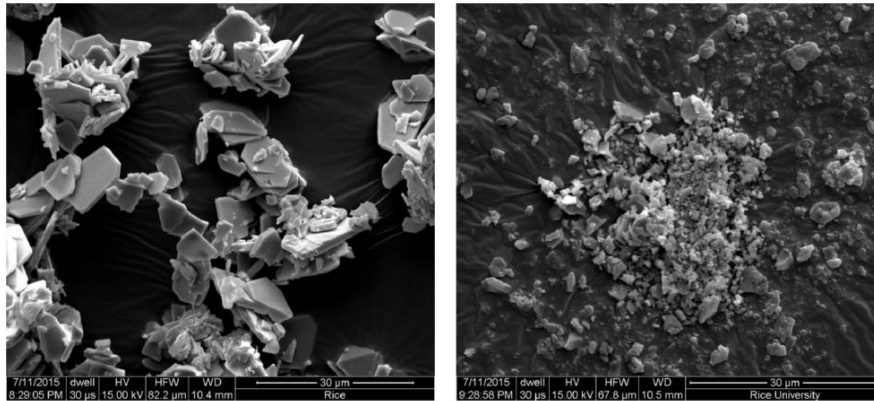


Figure 2. SEM image of barite crystals under laminar flow conditions ($Re = 176$, left) and turbulent flow conditions ($Re = 11249$, right). Image from (Yan, et al., 2016)

(Wang, et al., 2013) showed that positively charged ions have affinity to adhere to the negatively charged stainless steel surface. The adsorption of Ca^{2+} , Ba^{2+} and Si^{2+} onto the surface promotes adsorption of CO_3^{2-} , SO_4^{2-} and O^{2-} , thus, enhancing calcite, barite and silica nucleation on the surface. This means that these minerals 'prefer' to grow on a stainless-steel surface, rather than onto already existing deposition. An important result which follows from this cited experiment is that the initial mineral precipitation will fully cover the pipe wall, before it grows in height. This is also confirmed by (Hammer, et al., 2011).

(Tranter, et al., 2020) states that the solubility product of barite is highly sensitive to temperature: low temperatures correspond to a relatively low solubility product. Therefore, barite precipitates at lower temperatures, which occurs in the heat exchanger and downstream. Table 1 provides an overview of the mechanical properties of barite scales. These parameters affect the deposition dimensions and the resultant surface roughness. Data followed from (Wen, et al., 2020).

Table 1: Mechanical properties of barite. Data from (Wen, et al., 2020)

Mechanical properties barite	Value
Density [kg/m ³]	4480
Ultimate tensile strength [MPa]	6.4
Heat transfer coefficient [W/mK]	1.2

4 METHODOLOGY

In this chapter the methods and approaches used to model the different aspects of the two-way coupled hydro- and thermodynamic and geochemical scaling modelling workflow are discussed. In addition, it also provides the details of the uncertainty quantification approach used, and briefly discusses the different case studies the methods have been applied to.

4.1 SIMULATORS

Modelling of all flow related parameters (flowrate, pressure, temperature, etc.) are done using an in-house flow solver called Drift-Flux (Osipov, et al., 2014) which has been expanded with a connection to the geochemical speciation software PHREEQC and additional models for the calculation of deposition profiles and its effects on roughness and pressure drop within the system. Such a coupling can be done with any multiphase flow simulator which can calculate the process conditions, such as pressure, flow rates, temperature and gas-liquid fraction in geothermal plants.

The software PHREEQC is used to simulate the scaling potential of the geothermal brine related to temperature and pressure changes in the geothermal installation. PHREEQC version 3 is a computer program written in the C and C++ programming languages that is designed to perform a wide variety of aqueous geochemical calculations (Parkhurst & Appelo, 2013). Several thermodynamic databases are available for PHREEQC, which include the solubility constants of a set of minerals and gasses at a range of conditions that can be different for each database. For this study we selected the Pitzer database which is suitable for calculations of mineral and gas solubility at high salinity (downloaded with PHREEQC v3. <https://www.hydrochemistry.eu/ph3/index.html>). A disadvantage of this database is that it does not include aluminosilicates and only limited metals (sulphides), meaning that these compounds cannot be simulated with this database, even though they are commonly occurring scales.

4.2 COUPLED MODELLING WORKFLOW

Figure 3 gives a schematic overview of the different components included in the two-way coupled modelling workflow developed within this study. The modelling workflow has been developed to be applicable to different parts of geothermal systems (wellbores, heat exchanger system, etc.) or the complete geothermal doublet.

The workflow starts with the definition of the system geometry to be modelled, e.g. piping lengths, diameters, inclination, materials, and boundary conditions such as inlet temperature and pressure (reservoir conditions in case the entire wellbore is modelled). In addition, before the workflow can be executed, the composition of the geothermal brine has to be defined. Once all input parameters and boundary conditions have been defined, the system is discretized into a specified number of sections (cells), and the Drift-Flux model is used to calculate the flow properties (velocities, phase fractions), pressure, and temperature per cell. This model uses PVTsim (Anon., 2021), which takes the brine composition as an input, to perform any vapor-liquid equilibrium or fluid property calculations needed.

With the pressure and temperature in the system known, PHREEQC can be used to perform the geochemical speciation calculations, resulting in a certain amount of precipitate leaving the solution at each cell in the system. If this amount is non-zero, the composition of the brine is updated accordingly before the calculations of the subsequent cell are performed (thereby maintaining conservation of mass of each species in the brine).

After the amounts of precipitation per cell have been determined, the deposition and roughness models are used to calculate the change in inner diameter, roughness, and heat transfer of the pipe as a result of the newly formed scale layer. These updated values for diameter, roughness, and heat transfer are used in the next timestep to update the flow, pressure, and temperature in each cell, which in turn affects the precipitation amounts and diameters, roughness, and heat transfer of the next timesteps, and so on, completing the full two-way coupled interaction between hydro- and thermodynamics and geochemistry in the geothermal system.

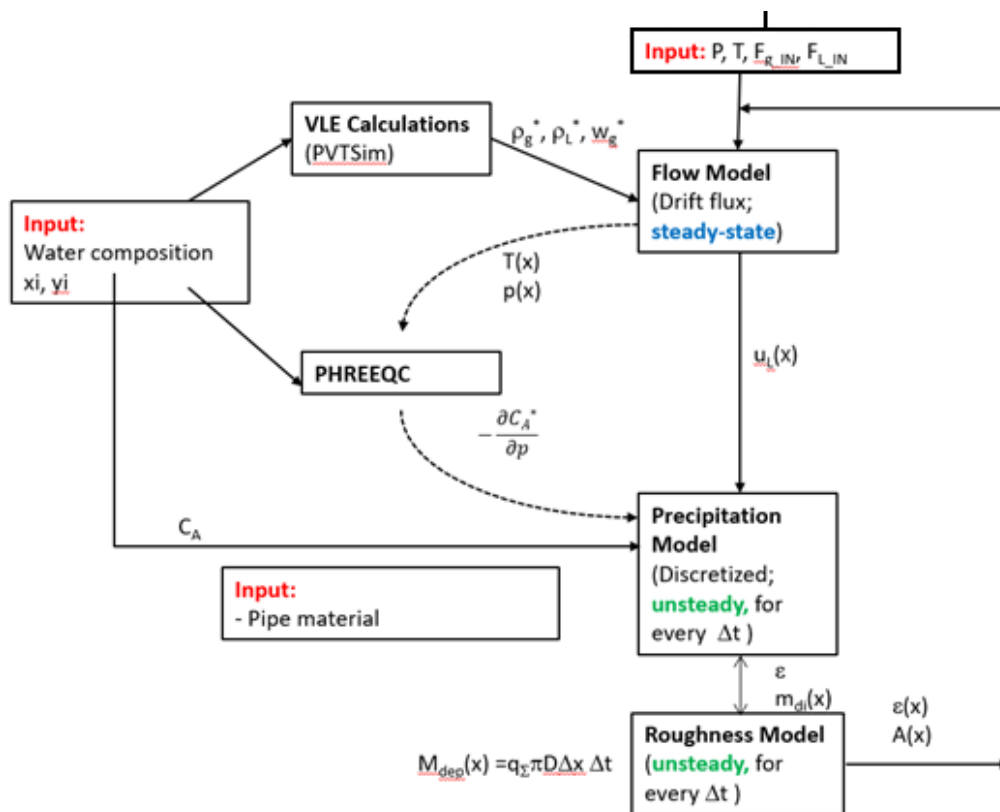


Figure 3. Workflow of the coupled flow-chemistry modelling framework. Image adapted from (Twerda & Veltin, 2014)

4.3 FLOW-PRECIPITATION INTERACTION

In this subchapter, the interaction between flow properties and mineral precipitation is explained. A precipitation model is created which describes the two-way coupling of the flow hydrodynamics with geochemistry (e.g. fluid composition).

The precipitation model relies on the following inputs:

- Aquifer/reservoir conditions: mineral concentrations, pressure, temperature.
- Geometry and properties of the geothermal doublet: pipe diameter, topside pressure, temperature drop in the heat exchanger.

The Drift-Flux code, incorporated in the precipitation model, uses aquifer/reservoir conditions and doublet geometry as an input and converts them to a pressure and velocity profile through the geothermal process plant. As barite is modelled in this report, the solubility of which depends primarily on temperature, only the heat exchanger and downstream piping are modelled as before the heat exchangers temperatures are higher and little barite is expected to precipitate. This section of the geothermal doublet is divided into 25 grid cells of equal length. The amount of grid cells chosen is not arbitrary: 25 grid cells ensure a fast computational speed, while also maintaining sufficient accuracy of local hydrodynamic- and thermochemical parameters. The precipitation quantity deviates less than 2 percent in comparison to an analysis of 100 grid cell, while the 25 grid cell analysis is 16 times faster. The brine temperature in the grid cells results from brine sampling from operators, and is interpolated between sampling points. After solving for the pressure and temperature at each grid cell, PRHEEQC is used to calculate the expected mass of mineral precipitation per cell.

Based on the literature discussed in Chapter 3, barite deposition can be modelled as conical structures along the pipe wall. (Wang, et al., 2013) and (Hammer, et al., 2011) stated that stainless steel pipes used in a geothermal doublet are negatively charged due to contact with the earth's crust. The core of the earth has a positive charge due to presence of extremely high pressures and temperatures. As a result, the earth's crust is negatively charged. Positively charged ions adhere to the pipe wall, which is further assisted by ion transportation from the bulk flow to the pipe wall due to turbulent flow (Schutte, 2016). Minerals therefore have a tendency to precipitate onto the pipe wall rather than on already existing precipitation layers. It is assumed that the pipe wall is completely covered with precipitated minerals after the first timestep. The geometry of the deposition of barite on a stainless steel surface is described by literature stated in Chapter 3, and it requires the calculation of the cone base width (shape of the deposition). For each cell, the mineral precipitation mass is converted into a cone width, which is equal for each cone in a single cell. This is illustrated in Figure 4.

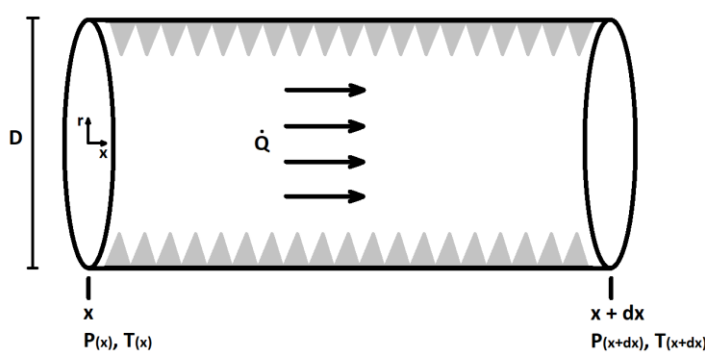


Figure 4. Illustrated view of the deposition profile of single grid cell

Here, the parameter D refers to the pipe diameter and parameter \dot{Q} refers to the volumetric flow rate. Dimensions of this profile are affected by the contact angle of the minerals with respect to the pipe wall, as well as the volumetric deposition along each individual cell. From the volumetric deposition and contact angle, the base and height of the triangular deposition model can be calculated for every cell. The accumulated crystals will experience a force due to the presence of the moving brine (shear stress between the deposited layer and fluid flow). An increase of crystal growth (increase in height of the deposition) leads to a reduction in effective flow diameter, which increases the force acting upon the minerals. The deposition can withstand a certain critical force, which is a function of the mechanical properties and the dimensions (most notably the cross-section) of the deposition layer. A critical deposition thickness (critical cone diameter) exists, where the fluid force exceeds the strength of the deposition, leading to destruction and transportation of the mineral above the threshold. This results in a trapezoidal deposition of the minerals along the pipe wall. The volumetric fraction of the deposition which is carried away by the flow is not analyzed further. The force diagram of one layer of scales is given in Figure 5.

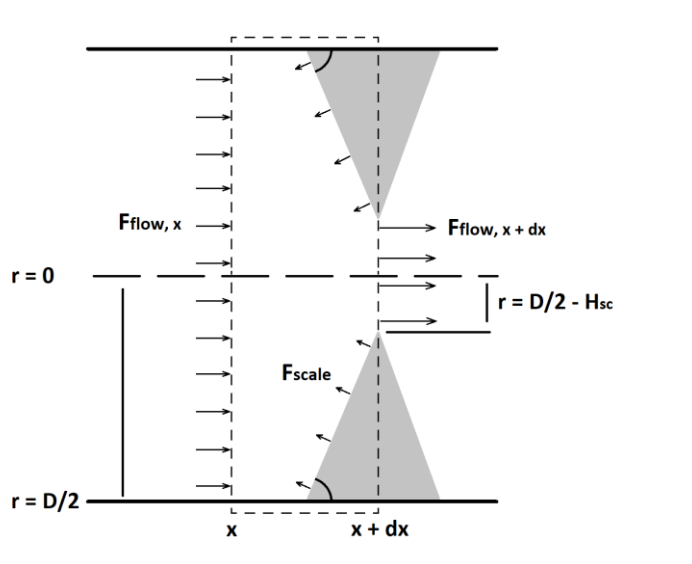


Figure 5. Force diagram of one layer of scales

Solving for the critical cross-section gives the desired deposition profile along the pipe wall. A trapezoidal structure will be formed. From this structure, the mean deposition height can be calculated. The cone height is discretized in N data points. The absolute and mean deposition height quantify the surface roughness per cell. (Bouزيد, et al., 2014) describes the surface roughness ϵ_{RMS} , based on the root-mean-square (RMS) method:

$$\epsilon_{RMS} = \sqrt{\frac{1}{N} * \sum_{i=1}^N (x - \bar{x})^2}$$

Where:

- ϵ_{RMS} is the surface roughness of the pipe due to mineral precipitation [m].

- N is the number of discretized data points which describe the height of a cone [-].
- x is the height of the cone at data point i [m].
- \bar{x} is the average cone height [m].

As the cones per cell are assumed to be identical, one cone is analyzed to obtain the surface roughness. The change in surface roughness imposes a change in the friction factor (f), described by (Haaland, 1983):

$$\frac{1}{\sqrt{f}} = -3.6 * \log_{10} \left[\frac{6.9}{Re} + \left(\frac{\epsilon_{RMS}}{3.7D} \right)^{\frac{10}{9}} \right]$$

Where:

- f is the fanning friction factor [-].
- Re is the Reynolds number [-].
- D is the pipe diameter [m].

An additional pressure drop will occur as a result of change of friction factor, described by (Mirmanto, 2013):

$$\Delta P_{cell} = f_{cell} * \frac{L_{cell}}{R - \bar{x}_{cell}} * \rho_{brine} * U_{cell}^2$$

Where:

- ΔP_{cell} is the pressure drop over a single cell [Pa].
- f_{cell} is the Fanning friction factor in a single cell [-].
- L_{cell} is the cell length [m].
- R is the pipe radius [m].
- ρ_{brine} is the brine density [kg/m³].
- U_{cell} is the flow velocity in a single cell [m/s].

The additional pressure drop affects the input pressure parameter of the next time step. The situation described above applies at the initial iteration, when no scaling is present in the cells. However, as more and more time steps are evaluated, more and more mineral will precipitate, and the deposition layer will increase in thickness. The deposition layer can be split into a constant thickness (resulting in a reduction in effective flow area) and a deposition roughness, described by the peaks which are on top of the deposition thickness. Due to the change in effective flow diameter and surface roughness, deposition may also occur at locations which were "scaling-free" beforehand.

(Dai, et al., 2021) and (Hammer, et al., 2011) performed experiments to evaluate “second-generation deposition” and concluded that the deposition profile remains roughly the same: it can be modelled as the same profile, with addition of a uniform thickness, corresponding to the scaling amount predicted by PHREEQC in the corresponding time interval. This is shown in Figure 6.

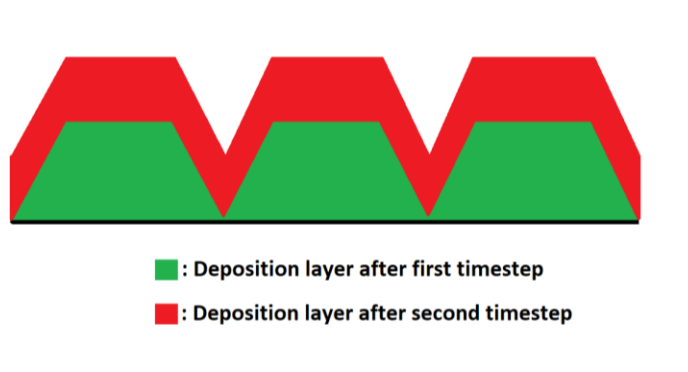


Figure 6. Illustration of the deposition layer, after one and two time step(s)

4.4 UNCERTAINTY QUANTIFICATION

As mentioned previously, the uncertainty in brine composition will lead to uncertainties in model outcomes which determine the confidence bounds of the prediction. For this reason, an uncertainty quantification workflow has been integrated with the modelling approach to estimate the magnitude of the effect of brine composition on flow conditions in a geothermal system. In this section, the type of uncertainties being studied is explained, and the uncertainty quantification approach is presented.

4.4.1 Types of uncertainty

As the name implies, uncertainty quantification (UQ) aims to quantify the impact of uncertainties on the outcome of a model of a physical system or experiment. In this, uncertainty is typically divided into two contributing parts: an aleatoric part and an epistemic (or systematic) part (Zhang, 2020).

Aleatoric uncertainties are uncertainties that are different each time an experiment is performed or vary continuously while a system is operated (Zhang, 2020). For instance, even if a ball is kicked with the exact same velocity and direction, natural (unavoidable) fluctuations in airflow around the ball and force transfer to the ball will mean that it never hits a target at exactly the same spot. Aleatoric uncertainties are often known as irreducible uncertainties.

On the other hand, epistemic uncertainties come from sources that in theory could be controlled, but for which it is difficult to do so in practice due to a lack of knowledge or information (Zhang, 2020). For instance, limitations in the understanding of a system might require simplified models that lead to uncertainties in predictions. Typically, epistemic uncertainties could be reduced by gaining better insights into the phenomenon at hand,

although again, this might not always be possible in practice. In short, aleatoric uncertainties come from the natural randomness of physical systems, while epistemic uncertainties arise from imperfections in our abilities to understand, control, or model them.

The uncertainty quantification in this work focusses solely on the effects of aleatoric uncertainty. More specifically, it focusses on the uncertainty in geothermal brine composition and how this affects the subsequent formation of mineral precipitates and ultimately the reduction in flowrates in the system over time.

4.4.2 Uncertainty quantification approach

The general uncertainty quantification approach used in this work is relatively straight-forward, and is summarized graphically in Figure 7. The method starts with a nominal brine composition for which the concentrations of different ions have been experimentally measured. Based on known measurement error bounds the possible upper and lower limits of the measurements are determined. Within these limits, a large number of brine compositions are sampled, and for each sampled composition, the relevant calculations are performed to get a distribution of a desired modelled quantity. For instance, in the example shown in Figure 7, the quantity of interest is the amount of barite precipitation. The resulting distribution can be further analyzed to find the expected deviations from the nominal and median values and identify best/worst case scenarios.

Brine compositions were sampled from a random uniform composition as well as using so-called Sobol sampling (Saltelli, et al., 2010). This latter sampling strategy was used to determine Sobol sensitivity indices for the different elements in the brine, which give an indication of which ions have the largest effects on the predicted quantity of interest (for more details, see the next subsection).

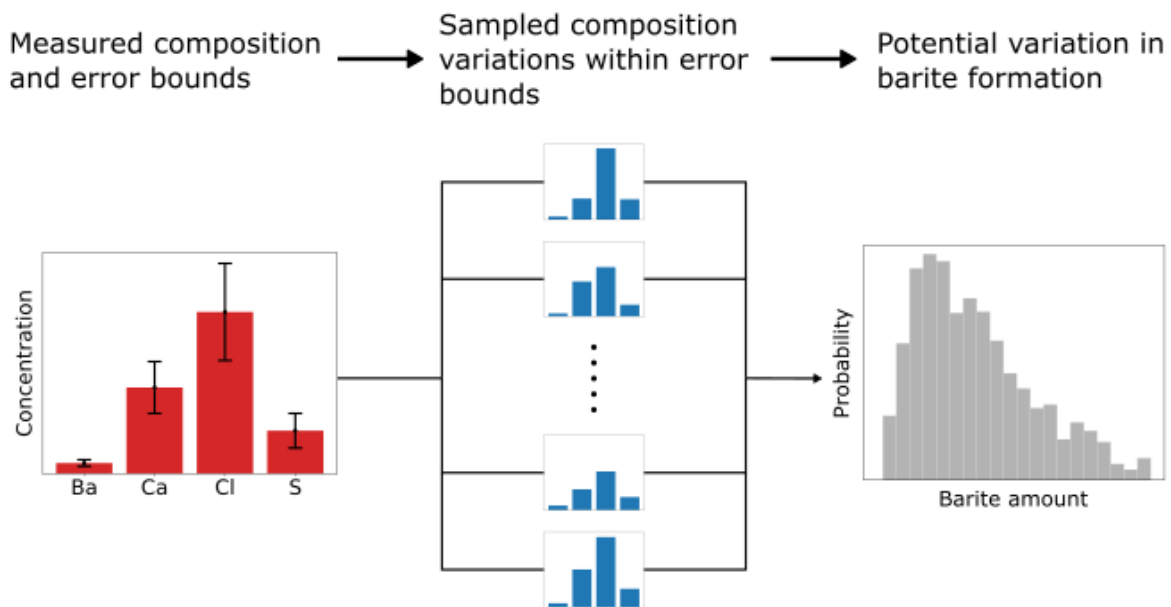


Figure 7. Graphical depiction of the uncertainty quantification approach

4.4.3 Sobol sensitivities

In addition to give an indication of the expected distribution of scaling at different brine conditions, uncertainty quantification (UQ) was also used to get an indication of which elements in the brine has the most impact on the scaling potential. In order to do so, the so-called Sobol sensitivity of the different brine elements that were varied during the UQ analysis were determined.

Sobol sensitivities are a variance-based approach, in which the magnitude of the impact of a given input parameter on the output is determined by evaluating how (much) the output changes when the input parameter is varied (Saltelli, et al., 2010). This impact is often divided into a specific set of "order" effects, e.g. first order, second order, and total order effects. First order effects look at the impact of varying a given parameter by itself, while second order effects vary the parameter along with one of the other input parameters to give an indication how their interaction affects the output (Saltelli, et al., 2010). As third or higher order effects become more and more difficult to evaluate, they are typically left out of analyses and the total order effect is calculated which summarizes all order effects of a given input parameters.

To increase the efficiency and accuracy of Sobol sensitivities, the Sobol sampling scheme is used to generate the model output samples from which the sensitivities are determined. Sobol sampling generates quasi-random samples which are more evenly distributed between the upper and lower bounds of the sampling limits (Saltelli, et al., 2010). Figure 8 gives an example of 256 samples sampled using either uniform random sampling or Sobol sampling and highlights the even distribution of Sobol samples.

The mathematics of how Sobol samples are generated and the sensitivities are calculated are considered outside the scope of this work, the interested reader is referred to (Saltelli, et al., 2010). The analyses in this work were performed using the "SALib" Python package (Herman & Usher, 2017).

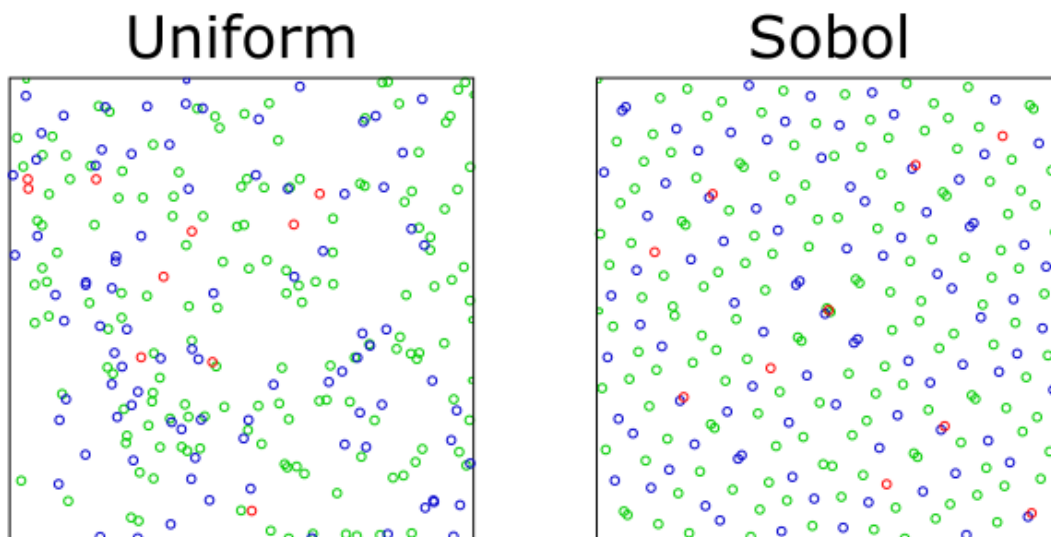


Figure 8. Example of samples generated using a (pseudo-)random uniform distribution (left) and a Sobol sampling strategy. Points in red correspond to the first 10 samples,

those in blue to the first 100 samples, and green the remaining samples. As can be seen, the Sobol samples are distributed more evenly throughout the sampling box

4.5 CASE STUDIES

The modelling approaches developed in this task were applied to three different case studies of increasing complexity, through integrating more of the different sub-models. In this section, each of the cases are briefly explained. All case studies focused primarily on the scaling of barite within heat exchanger equipment (specific geometry and boundary conditions are discussed in Section 5.3). Brine compositions were based on measurements from a geothermal doublet in the Netherlands (details given in Section 5.1 and 5.2).

4.5.1 Case A: barite scaling modelling

In this case study, the PHREEQC model used to estimate barite precipitation potential under at different conditions was developed. In addition, using this model, the temperature-dependency, kinetics, and effects of other ions/minerals on barite precipitation were investigated.

4.5.2 Case B: uncertainty quantification of scaling potentials

Initial uncertainty quantification activities focused solely on the impact of uncertainty in brine composition on the amount of potential scaling at a singular operating condition (i.e. a single combination of pressure and temperature). This case did not include any deposition or roughness modelling, and as such did not contain the full two-way coupling between hydrodynamics and deposition modelling.

4.5.3 Case C: modelling the impact of hydrodynamics on scaling precipitation

In the third case study, the modelling activities were expanded to the calculation of the height and profile of the deposition layer and roughness based on the scaling amounts and flow within the heat exchanger system. Activities in this case study also included the addition of the two-way coupling between hydrodynamics and scaling. However, it did not include any uncertainty quantification.

4.5.4 Case D: uncertainty quantification of scaling precipitation, roughness, and flow

The final case study combined all workflows that were previously developed, i.e. the full two-way coupling of hydrodynamics and scaling under uncertainty in brine composition, and applied them to the same heat exchanger system as the prior case.

5 RESULTS

In this chapter, the outcomes of the modelling work as applied to the case studies described in Section 4.5 are given. The results start with the description of the geochemical models and the initial model results for barite scaling as affected by key parameters. Secondly, the initial analysis of the impact of uncertainty in brine composition on the scaling potential of barite, followed by the description of results from the two-way coupling approach, and end with the outcomes of the full workflow combining the uncertainty quantification with the two-way coupled models.

5.1 RESULTS CASE A: BARITE SCALING MODEL

5.1.1 Model set-up and initialization

The geothermal fluid is a combination of brine and gas (together with solid particles) which are analyzed and characterized for their compositions in the laboratory. The gas and liquid compositions used in this section are given in Table 2 and Table 3 respectively. As part of this work was executed after initial work on the uncertainty quantification and coupled modelling, the brine composition is slightly different from that given later as additional measurements had been analyzed leading to updated concentration values.

In order to input the characterized fluid composition to PHREEQC, the brine ('SOLUTION') and gas ('GAS_PHASE') are combined at reservoir pressure and temperature to approximate the composition of the reservoir fluid. For this case study, one specific brine and gas composition is selected. A gas water ratio (GWR) of 0.36 is used for the gas volume. The gas composition is listed in Table 2. Any charge imbalance of the fluid (e.g. due to not including all the metal compounds with the Pitzer database) are solved by adjusting the sodium concentration with the 'charge' function. The fluid and gas are combined at 105 °C and 331 bar. Due to the dissolution of CO₂ into the brine, the pH of the resulting reservoir fluid decreases from 5.2 to 4.8. Under these conditions the barite saturation index is -0.3, indicating that barite is slightly undersaturated in the reservoir. The effects of uncertainties in sampling and measurement on the saturation index of barite and resulting precipitation will be addressed with the uncertainty assessment workflow in section 5.2.

The reservoir fluid defined with PHREEQC can subsequently be exposed to any temperature or pressure condition in the geothermal installation for geochemical calculations of scaling potential which will be discussed in the following sections. First equilibrium barite precipitation will be assessed followed by the incorporation of kinetics in the model. Secondly, the effect strontium, calcium and magnesium on barite scaling prediction will be assessed.

Table 2 Gas composition of the case study fluid

Gases	Mole fraction
CO₂(g)	0.25659
Methane(g)	0.57209
Nitrogen(g)	0.10556

Table 3 Brine composition of the case study fluid

Element	Concentration (mg/l)
Na	89000
K	810
Ca	9500
Mg	1200
Ba	5.3
Sr	440
Fe	124
Cl	160000
S(6)	390
C(4)	17.7
Mn	10.3
Li	31.1
Si	9.37

5.1.2 Barite scaling potential

Since barite precipitation is strongly controlled by temperature, this case study is focused on precipitation with cooling in the heat exchanger. A fixed top-side pressure of 10 bar is assumed, allowing minor amounts of gases to exsolve. The first models were run assuming instantaneous (equilibrium) reactions. Figure 9 shows the predictions of increasing barite precipitation with lower temperatures. At a cooling temperature of 30 °C the predicted amount of barite scaling is 3.3E-5 mol/kgw.

A second PHREEQC model was made for kinetically controlled mineral precipitation using a rate expression described by (Lasaga, et al., 1994). The rate expression describes the time required for a mineral to precipitate and to reach equilibrium as dependent on several parameters such as the saturation index and a mineral specific reaction rate. The barite reaction rates are taken from (Palandri & Kharaka, 2004). The kinetic model was run with a fixed pressure and temperature of 10 bar and 30 °C in several time steps for a specific time interval. Figure 10 shows that after approximately 4 years, the fluid composition approaches equilibrium with respect to barite at the new temperature of 30 °C. Considering that the residence time of the fluid in the geothermal system (plant) is a matter of minutes and not years, the amount of predicted barite scaling will be significantly reduced when taking reaction rates into account. Running the kinetic model for ten minutes yields 7.70E-10 mol/kgw barite scaling (Figure 11), instead of the 3.3E-5 mol/kgw barite predicted with the instantaneous equilibrium model (Figure 9). This illustrates the large effect of kinetics on predicted mineral precipitation.

These results indicate that caution is advised when assessing the barite precipitation with instantaneous ('in equilibrium') simulations without considering reaction rates, as will be initially done for the workflow development in the following case studies. For barite this may significantly overestimate precipitation. Furthermore, including the kinetic rates will most probably spread-out barite precipitation through the geothermal installation and injection well, maybe even down to the reservoir. Barite precipitation may not even be predicted at all following the theory that barite precipitation starts only in case of significant mineral oversaturation. Some studies (e.g. (Kristensen, et al., 2020), (van der Hulst, 2019)) argue that it is unlikely that barite scale will cause problems at Saturation Index (SI) values lower than 1 or even 3. Figure 12 shows the calculated saturation index of barite with cooling (when barite precipitation is not allowed in the model). For our case, the saturation index is below 1 for 30 °C and only exceeds a SI value of 1 after cooling to 20 °C (Figure 12). Our model results, which show a large kinetic control and a SI below 1, agree with the lack of observed barite scaling in Dutch doublets (which cool to temperatures between 30 and 40 °C).

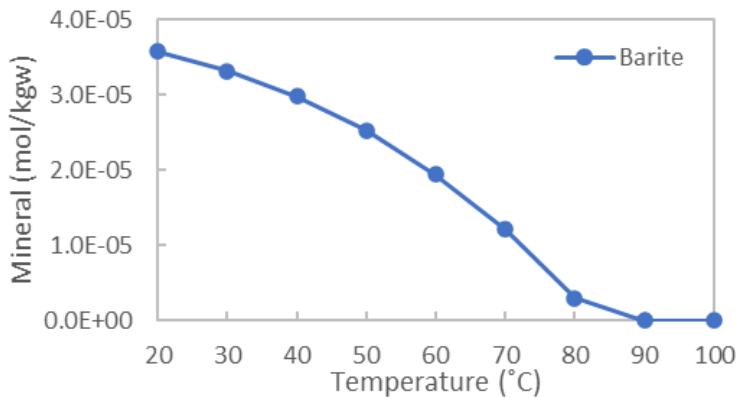


Figure 9. Barite precipitation simulated for cooling from 100 to 20 °C

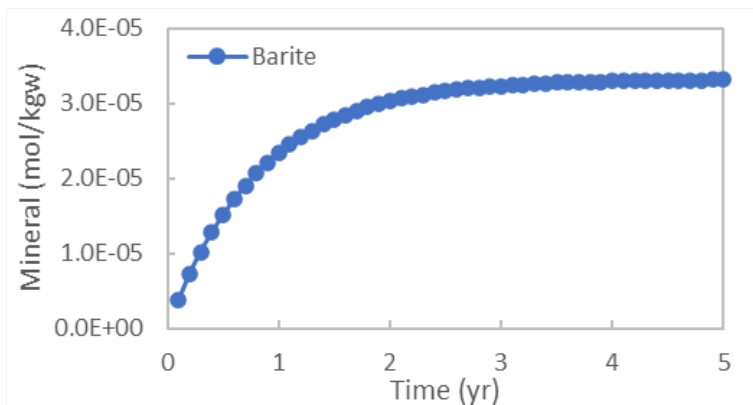


Figure 10. Kinetic barite precipitation at fixed conditions of 30 °C and 10 bar, simulated for a time span of 5 years

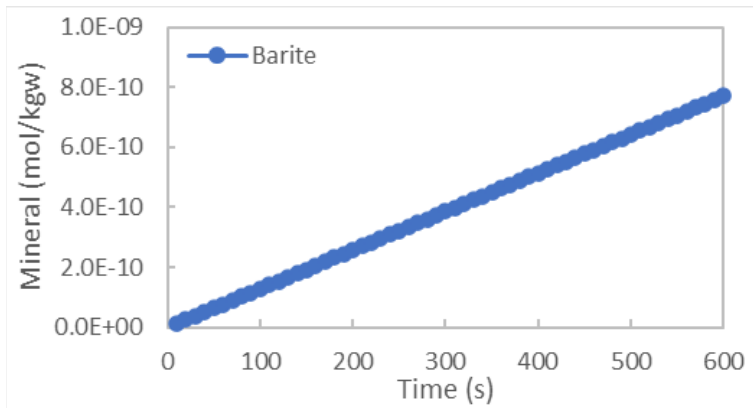


Figure 11. Kinetic barite precipitation at fixed conditions of 30 °C and 10 bar, simulated for a time span of 10 minutes

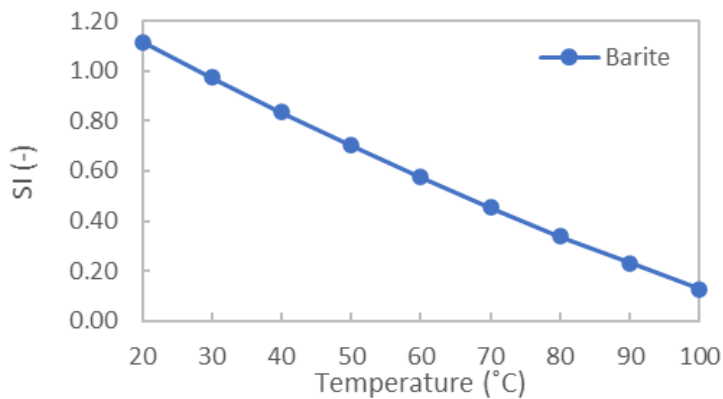


Figure 12. Barite saturation index (SI) simulated for cooling from 100 to 20 °C

5.1.3 Effect strontium on barite scaling potential

Similar to barium in barite, strontium can form a sulphate mineral (celestite or celestine). Barite and celestite can form a solid solution which is observed in samples of geothermal scales (e.g. (Haas-Nüesch, et al., 2018), (Heberling, 2017), (Regenspurg, et al., 2014)). The fluid of this case study contains a very high strontium compared to the barium concentration (Table 3), which suggests a potential for combined celestite and barite precipitation. Studies on natural samples of barite and celestine indicate a slightly non-ideal regular solid solution with a dimensionless interaction parameter a_0 (or Guggenheim parameter) in a range of $1.6 < a_0 < 2.0$, assuming no miscibility gap in the solid-solution series ((Monnin & Cividini, 2006) and (Heberling, 2017)). We used a nondimensional Guggenheim parameter of 1.8 for the solid solution in PHREEQC.

Figure 13 shows the amount of barite and celestite precipitating together as solid solution. At the onset of cooling, the scale becomes increasingly celestite rich. Only at 30 °C and lower, barite is the dominant component. This is probably the reason why barite is a common scale mineral, assuming that cooling is fast and the brine mostly experiences a low temperature. The incorporation of strontium in barite reduces the total predicted scaling to $1.9E-5$ mol/kgw, compared to the $3.3E-5$ mol/kgw of pure barite. This indicates that the high strontium concentration in the fluid and incorporation of strontium in barite might reduce the scaling potential.

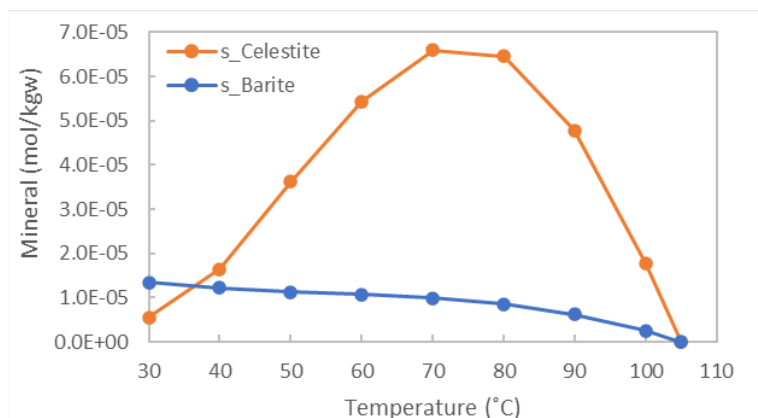


Figure 13. Precipitation of a barite-celestite solid solution, simulated for cooling from 105 to 30 °C.

5.1.4 Effect calcium and magnesium on barite scaling potential

Barite precipitation is controlled by several parameters as mentioned previously. In literature, calcium is reported to have a large effect on barite solubility. Barite scaling has been reported to be more favorable for calcium rich geothermal fluids (Kristensen, et al., 2020). This could be related to a decrease in ion pair stability with decreasing temperature by a factor of ~ 3 from 150 to 25 °C (Dai, et al., 2014), meaning that the ion pair would disassociate upon cooling, increasing the concentration of free SO_4^{2-} . This causes barite solubility to be substantially affected by temperature changes in Ca-rich brines (Kristensen, et al., 2020). In contrast, experimental work showed that the precipitation kinetics of barite are affected by an inhibitory effect of calcium ions which can adsorb on barite nuclei during formation and growth (Jones, et al., 2004); also, the formation of the calcium sulfate ion pairs CaSO_4 decreases the free sulfate, hence the saturation state of the solution (Azaza, et al., 2017). Thus, increased calcium cations in solution would reduce precipitation and nucleation rates due to the lower supersaturation and higher solubility of barite. In the literature (Jones, et al., 2004) it was also discussed the disagreement in literature on the effect of calcium on barite precipitation, either promoting or inhibiting its precipitation. For example other controls on barite precipitation could interfere with interpreting results such as the presence of organic additives or the effect of the changed ionic strength of the fluid with varying calcium concentrations. For our study, the theoretical effect of calcium on barite precipitation will be assessed with PHREEQC.

For this case study, the effect of the calcium concentration on barite solubility is assessed by running the cooling simulation with different initial calcium concentrations. Sodium is used to charge balance the initial solution with the new calcium concentration and hence the ionic strength of the fluid has not changed. Figure 14 shows the reduction of predicted barite scaling with higher calcium concentrations, due to an apparent increased solubility. With increased calcium, more cooling is required for barite scaling to start, but the difference in barite scaling becomes less pronounced at lower temperatures. The simulated decrease of barite scaling agrees with the findings of (Azaza, et al., 2017) and (Jones, et al., 2004), of reduced precipitation rather than an increased scaling risk for calcium rich brines.

The same variation in concentration was investigated for magnesium to check whether other elements could have a similar effect on simulated barite precipitation. The magnesium concentration does not have a significant effect on the barite solubility and predicted precipitation (Figure 15).

The results indicate that the model and the thermodynamic database are able to capture specific interactions of calcium, barium and sulphate while other cations are of much less influence. In the following section, the effects of uncertainties and variations in fluid composition on barite precipitation will be further discussed.

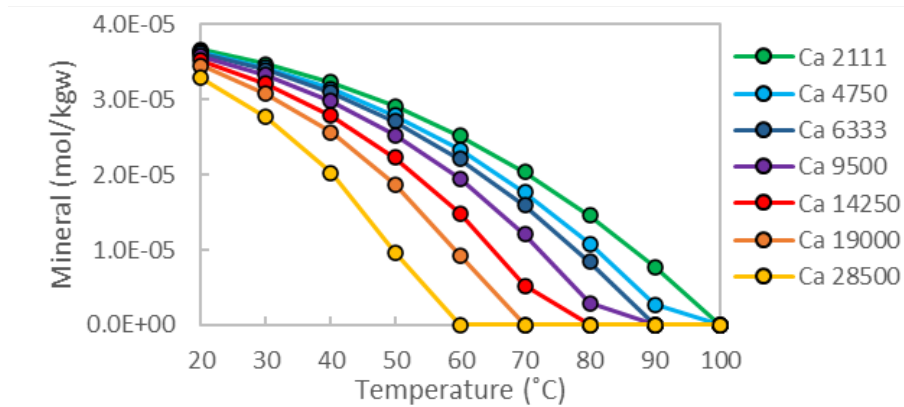


Figure 14. The effect of different initial calcium concentrations in mg/kg-water on barite precipitation, simulated for cooling from 100 to 20 °C.

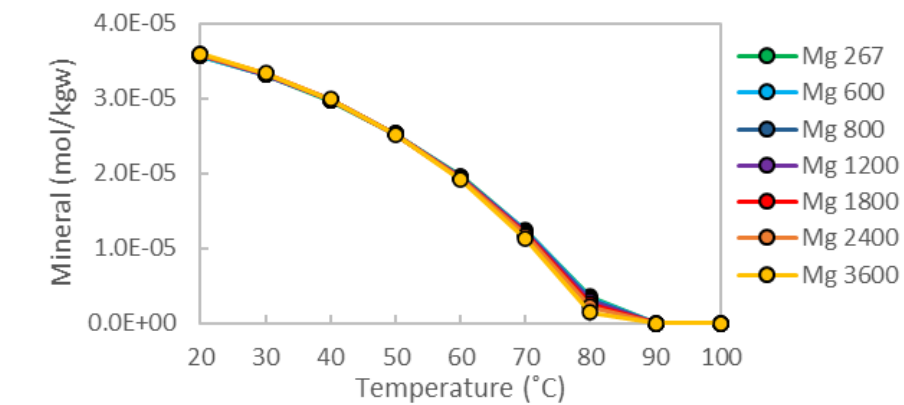


Figure 15. The effect of different initial magnesium concentrations in mg/kg-water on barite precipitation, simulated for cooling from 100 to 20 °C.

5.2 RESULTS CASE B: IMPACT OF UNCERTAINTIES ON SCALING POTENTIAL

To investigate the impact of uncertainties in the geothermal brine solutions that come from element concentration measurements or arise from natural changes to the geothermal system, the uncertainty quantification approach as described in Section 4.4 was applied to the modelling of barite scaling at a fixed temperature-pressure combinations.

5.2.1 Brine composition and uncertainty bounds

An initial analysis was done on the fluid composition data using REFLECT project database for a single well (multiple measurements from a single well) and a group of wells from the same formation. In the second case, the impact of measurement uncertainties and variabilities in the ions compositions are combined. The result of the initial analysis is shown in Figure 16. The analysis shows that the largest uncertainties in the fluid compositions are in iron, nickel and aluminum which are unlikely to impact the barite precipitation. However, the impact of even a small variation/uncertainty in the other ions on barite or other mineral precipitation is still unknown.

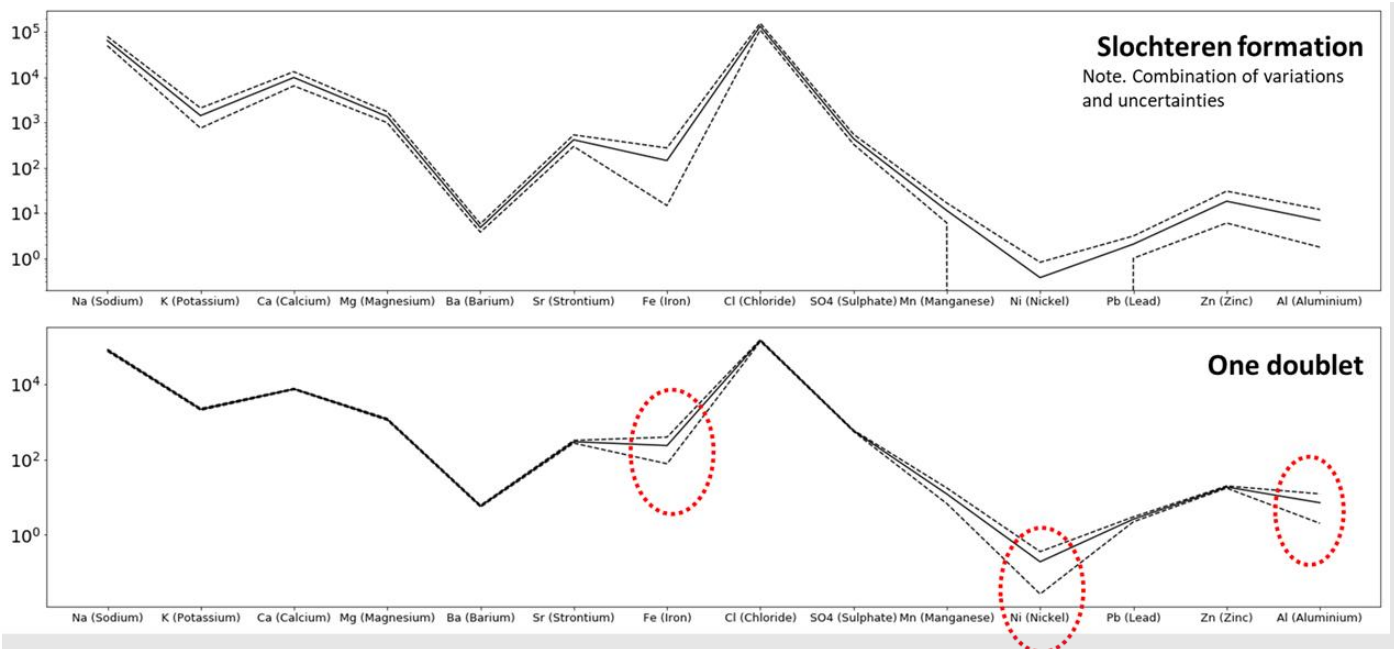


Figure 16. Uncertainties in the fluid composition measurements (in mg/L) for a group of wells in a formation (top) and a single doublet in the same formation (bottom), the solid line indicates the mean value and the dashed lines are the standard deviation

For this purpose, in total eight elements were taken into account during the uncertainty quantification, including: barium (Ba), carbon (C), calcium (Ca), chlorine (Cl), potassium (K), magnesium (Mg), sodium (Na), and sulphur (S). The nominal concentrations and maximum/minimum variation of these elements were based on downhole sample measurements of the brine composition at a Dutch geothermal doublet. The upper and lower bounds between which brine samples were generated were calculated from these percentages.

Two different variation magnitudes were considered: smaller “well variations” which were representative to the uncertainties in a single well, and “formation variations” which represented the much larger variations between wells within the same geological formation (Slochteren formation). All nominal concentrations and maximum/minimum deviations from it are listed in Table 4. Please note that this analysis was performed before those of Section 5.1, which uses more recent measurement values. Thus, there is a difference between the concentrations reported in Table 3 and Table 4.

Table 4. Nominal concentrations and minimum and maximum percentual deviations of elements included in the brine uncertainty quantification analysis

Element	Nominal Concentration (mg/l)	Minimum/maximum percentage deviation	
		Variation in well	Variation in formation
Ba	5.5	±3%	±30%
C	0.001	±3%	±30%
Ca	7450	±3%	±30%
Cl	145000	±3%	±30%
K	2200	±0.5%	±5%
Mg	1150	±4%	±40%
Na	85000	±2%	±20%
S	585	±4%	±40%

5.2.2 Uncertainty in barite scaling potentials

Approximately 10,000 samples were generated (number depends on the number of parameters included in the analysis and the specifics of the Sobol sampling scheme) based on the uncertainty bounds from well and formation variation. For each sample a PHREEQC simulation was performed to calculate the barite scaling amounts. Figure 17 shows the calculated barite scaling amounts for both variation scales. The most noticeable difference is the width of the respective distributions (bottom plots), which, as expected is very narrow for the smaller variation, and broad for the larger variations. For the uncertainties based on well variations, the mean value for the barite precipitation is significantly higher than that for the formation variations and lies around one standard deviation away from the mean of the formation variations. Moreover, when comparing both distribution means to the nominal value (purple dash-dotted line) the well variations show only minor deviations (0.7% lower mean than nominal value), while the formation variation mean is around 20.7% lower. This is likely due to another significant difference: the fact that for the larger variations, there are a considerable number of brine compositions for which there is no barite scaling predicted at all. Not only does this lead to a large “tail” towards the lower amounts of barite precipitation in the formation variations and resulting lower mean, but it will also significantly impact the flow profile in the geothermal system (something investigated in more detail in Section 5.4).

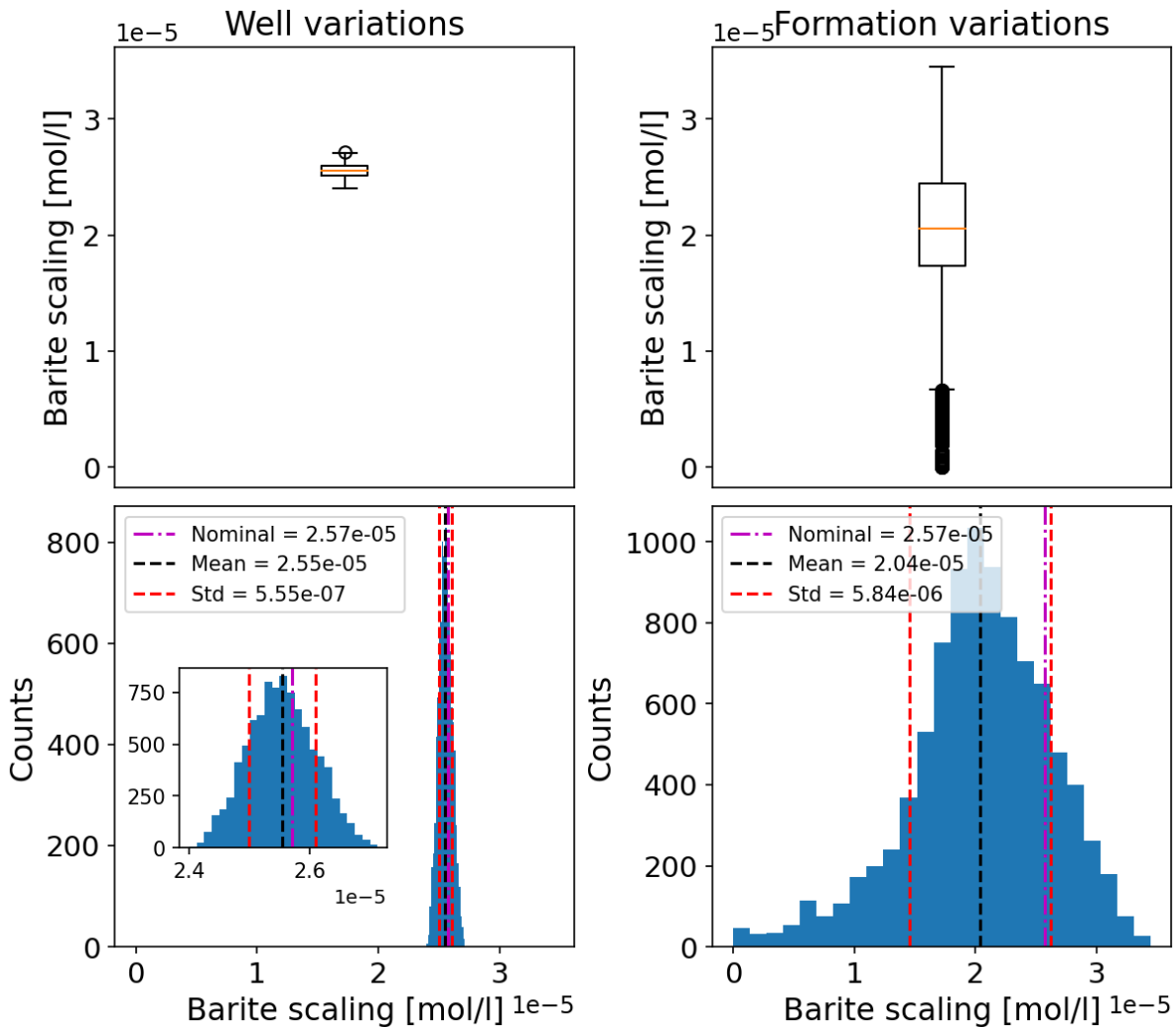


Figure 17 Barite scaling amounts calculated using PHREEQC at 70 °C and 10 bar for the smaller well variations (left), and larger formation variations (right). Results are plotted both as a box plots (top) and histogram plots (bottom). The black dashed lines indicate the mean value of barite scaling distribution, red lines dashed lines are one standard deviation away from the mean, and the purple dash-dotted lines indicate the barite scaling amount corresponding to the nominal brine composition

In addition to the barite scaling amount distributions shown in Figure 17 for a temperature of 70 °C and pressure of 10 bar, Figure 18 shows the distributions at five other temperature-pressure combinations representative of different points within a heat exchanger. In this case, distributions are only determined for the formation variations.

As can be seen, as the temperature changes, so do the barite distributions. While at higher temperatures, where the solubility of barite is high, there is a large amount of possible brine compositions that result in no precipitation, this slowly changes as the temperature drops and solubility decreases. Eventually, at the lower temperatures (50 degrees and below), barite is expected to precipitate regardless of the brine composition, although there is still a lot of variance in the potential amount of barite that precipitates. Looking at the nominal values for each points, we see that all of them predict barite scaling to occur. Comparing them to the

mean of the distribution, the largest differences are found at the higher temperatures, with a maximum difference of 46% at the first point, which reduces at the last point to a difference of around 13%. These results are due to the large number of samples for which no barite scaling is predicted, which lowers the mean of the distribution significantly.

From the analysis it can also be seen that 70 °C seems to be the point around which the possibility of barite precipitation goes from a small chance of no precipitation at all, to certain precipitation no matter the brine composition (which is consistent with Figure 9). Thus, while the largest effects of uncertainties in absolute terms are found at lower temperatures, since they have broader ranges of potential scaling amount values associated with them, the uncertainty in whether scaling occurs or does not occur are found at higher temperatures (70 °C and above). When it comes to heat exchanger performance, these latter uncertainties are expected to play a larger role, as the difference between no precipitation at all to some precipitation has quite a large impact on the flow and heat transfer within the system (mainly due to a change in wall roughness and the addition of thermal resistance due to the barite deposition layer, as will be shown in Section 5.3).

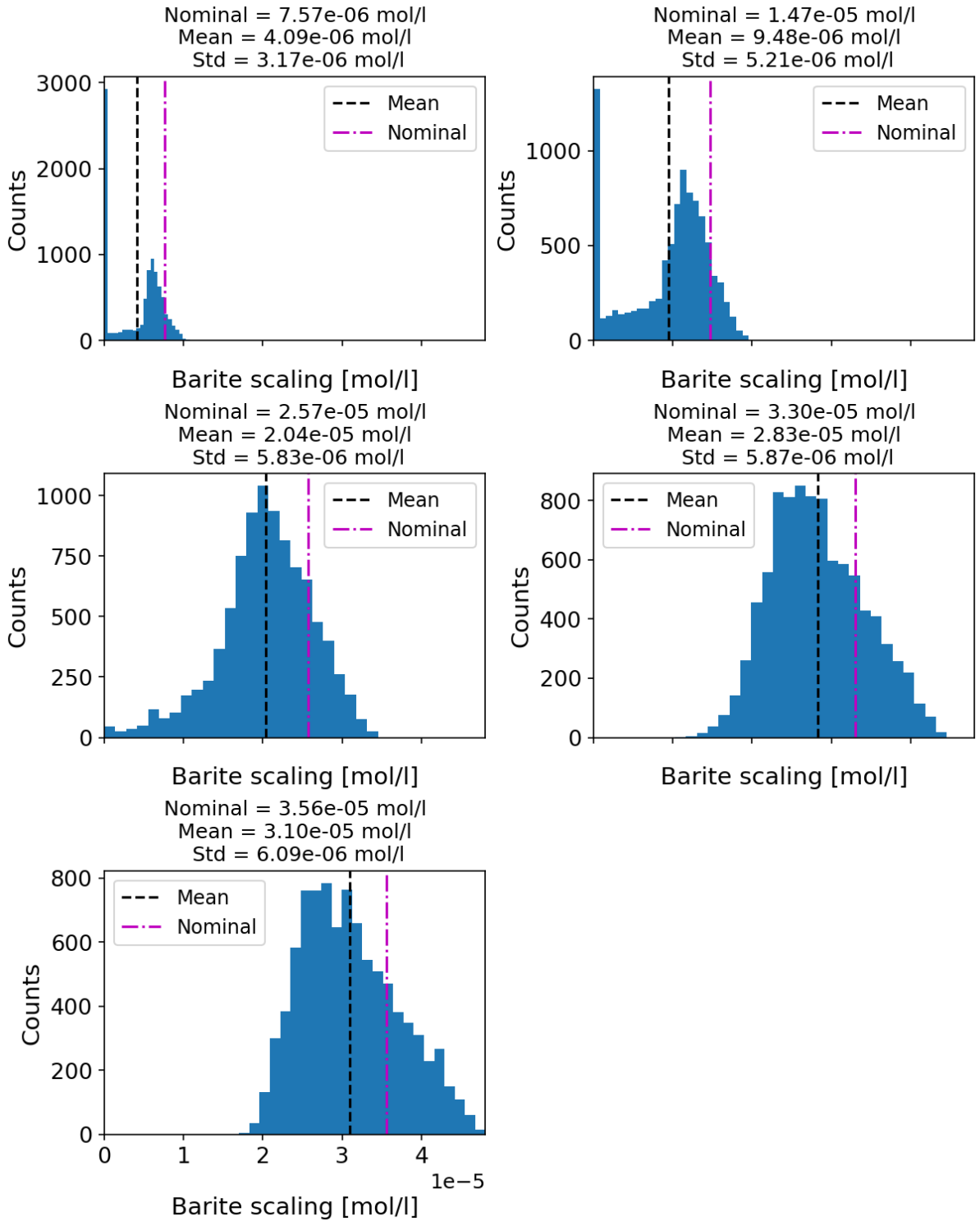


Figure 18 Barite scaling amount distributions at five different temperature-pressure combinations (from top to bottom, left to right: 100 °C, 10 bar; 90 °C, 8.75 bar; 70 °C, 7.5 bar; 50 °C, 6.25 bar; and 40 °C, 5 bar). The black dashed lines indicate the mean value of barite scaling distribution and the purple dash-dotted lines indicate the barite scaling amount corresponding to the nominal brine composition

5.2.3 Sobol sensitivities of barite scaling potential

In this task, Sobol sensitivities were used to get an indication of which extent the eight elements included in the uncertainty quantification have the biggest impact on barite scaling. This information can then in turn be used to limit the number of elements to be included in later analyses, reducing the number of samples required, and improving the efficiency of the complete workflow.

Figure 19 shows the first, second, and total order Sobol sensitivities of each of the eight elements included in the brine composition uncertainty analysis, both for the well variations (left) and formation variations (right). As can be seen, for both variation magnitudes, four of the elements stand out as having a significant impact on the outcome (barium, sulphur, calcium, and chlorine), while the other four (carbon, potassium, magnesium, and sodium) have negligible to no importance. These findings, especially the high second order effect of the combination of Barium and Sulphur, align closely with what would be expected from the chemistry of barite precipitation. Barite itself is a compound of barium and sulphate, and thus its formation primarily depends on the presence of the elements making up these two ions. According to Tranter et al (2020), the ratio between sulphate and barium is an important control on the amount of scaling that can be expected, with less precipitation if the initial ratio deviates more from unity. In addition, calcium and chlorine have been known to affect the formation of barite (as discussed in Section 5.1.4), which explains the additional minor sensitivities to those elements.

Another interesting result is the changes observed when going from smaller well variations (plots on the left) to the larger formation variations (plots on the right). While the four most important elements remain the same, the magnitudes of their sensitivities change considerably. Especially those of barium and sulphur show interesting changes. Where for the smaller variations sulphur had by far the highest impact on the outcomes, for the larger variations barium becomes the element to which the barite formation is most sensitive. This seems to indicate that when looking at small potential measurement errors, it is more important to limit the uncertainty in sulphur, while for large possible uncertainties, it is better to limit the potential error in barium. The analysis also shows that going forward, carbon, potassium, magnesium, and sodium can be left out of consideration during any uncertainty quantification related to barite modelling.

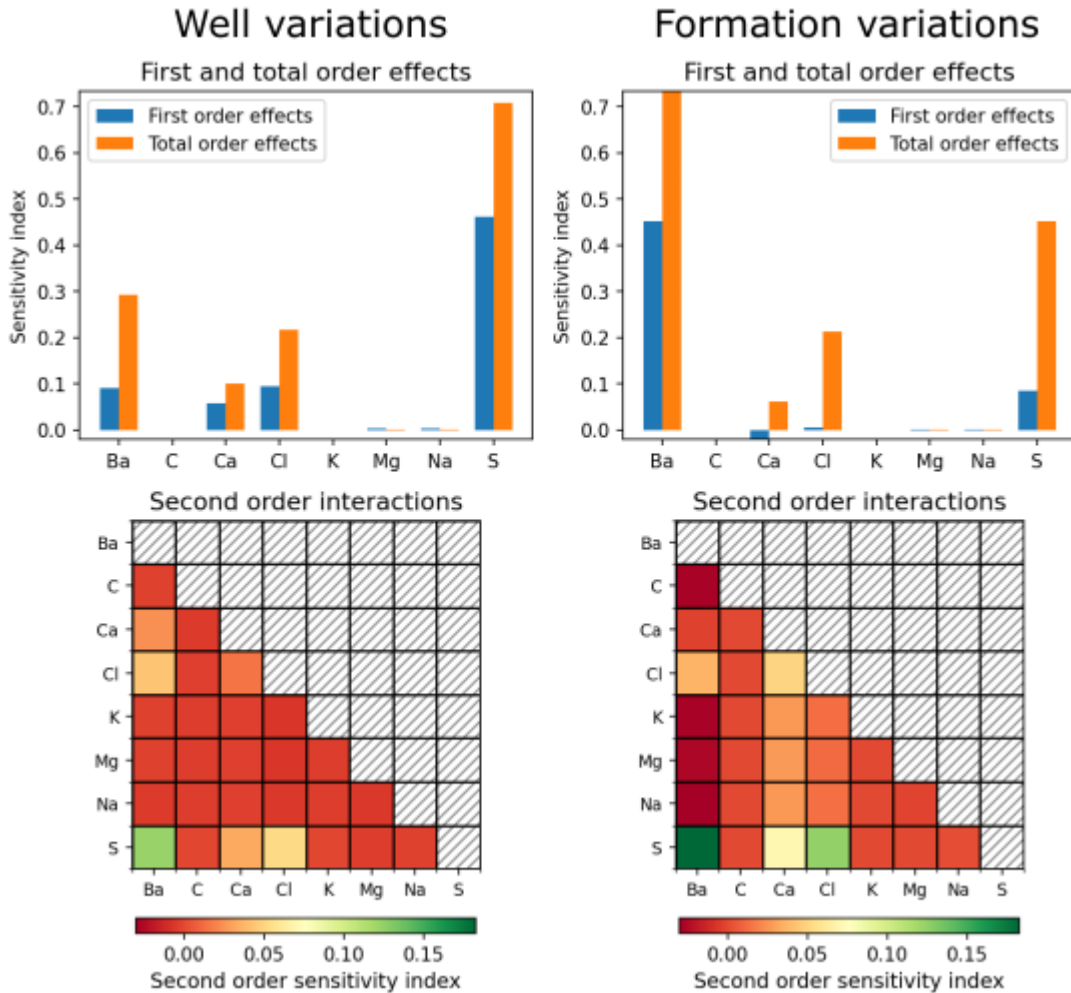


Figure 19 First and total order Sobolj sensitivities (top) as well as second order sensitivities (bottom) for the eight elements included in the brine uncertainty quantification for the smaller well variations (left) and larger formation variations (right)

5.3 RESULTS CASE C: IMPACT OF HYDRODYNAMICS ON SCALING

In this section, the effects flow, pressure, and temperature have on the amount and profile of scaling deposits of barite are given. It also discusses how these deposits affect inner pipe diameters and roughness of pipe walls and how these parameters themselves in turn affect flow profiles and heat transfer within the system.

These calculations focused on the modelling of a single heat exchanger pipe of length 3.4 m with an inner diameter of 0.01 m discretized into 25 cells. The inlet and outlet temperature of the pipe were 100 °C and 40 °C respectively, and inlet pressure was set to 10 bar. Flow was modelled as a single-phase liquid.

5.3.1 Deposition profile

As stated in Section 4.3, barite deposits in conical shapes along the pipe wall. The top of the cones gets sheared off due to hydrodynamic forces imposed by the transported brine. A shear stress force balance is constructed and used to calculate the critical deposition height where

the shear stress experienced by the deposition exceeds the ultimate tensile strength of the precipitated mineral.

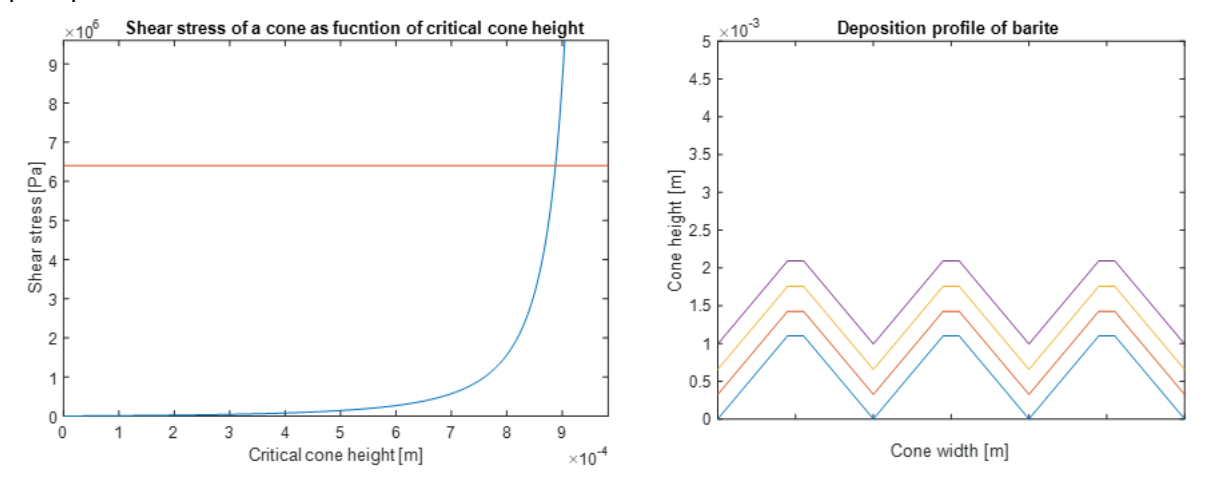


Figure 20. Shear stress as a function of critical cone height (left) and deposition profile of barite over time (right).

The result is a trapezoidal deposition profile (in 2D). As time progresses, the thickness of the deposition layer grows, the roughness/resistance of the pipe flow increases and eventually the effective flow diameter reduces. This results in larger hydrodynamic forces, which impact the force balance on the cones: the critical height of the cones (with respect to their total height) reduces, resulting in trapezoidal structures which are more flat. The root-mean-square error thus decreases with increasing deposition thickness, which results in lower surface roughness. This affects the flow regime, leading to (local) pressure changes over time, which impact the scaling tendency.

5.3.2 Flow velocity profile and average flowrate

Deposition dimensions per cell result in an additional pressure drop in each cell. Brine pressure in the pipe decreases as the brine progresses through the pipes, because pressure differences causes fluid transportation. Cells without precipitation have a base pressure drop, which is a function of hydrodynamic properties (operating pressure of the doublet) and doublet properties (surface roughness of the stainless steel pipe, grid cell length). Precipitation which is present in a cell results in an additional pressure drop: the combination of the base pressure drop and additional pressure drop due to scaling gives the total pressure drop over a cell.

The additional pressure drop can play a role in two manners: a pressure drop induced by the surface roughness of the deposition layer and a pressure drop induced by the reduction in effective flow area. Minerals which precipitate on a surface, such as barite, have the tendency to precipitate on the pipe wall first, before growing inward over time, and as time progresses, the deposition layer grows by means of a total deposition thickness increase (Hammer, et al., 2011). The surface roughness induced by mineral precipitation also changes slightly over time: the hydrodynamic forces which act on the scales gradually increase as the effective flow area decreases, which results in larger tensile strength in the cones, causing them to shear off at lower heights, which reduces the trapezoidal height and subsequent roughness value. Results show that the pressure drop in cell 4 (the cell with the largest precipitation volume) after the

first timestep of 25 days is equal to 18.1 mbar, including the surface roughness pressure drop of 12.5 mbar, which is 69 percent of the total pressure drop. However, after 100 days, the pressure drop in cell 4 has risen to 47.0 mbar, while the surface pressure drop decreased to 11.7 mbar, which is 25 percent of the total pressure drop. Therefore, the pressure drop due to reduction in effective flow area outweighs the pressure drop induced by surface roughness as longer time periods are evaluated.

By means of superposition, the total pressure drop is calculated and converted to the flow velocity reduction profile and a volumetric flowrate reduction over time (trend data), which are shown in Figure 21 and Figure 22 respectively.

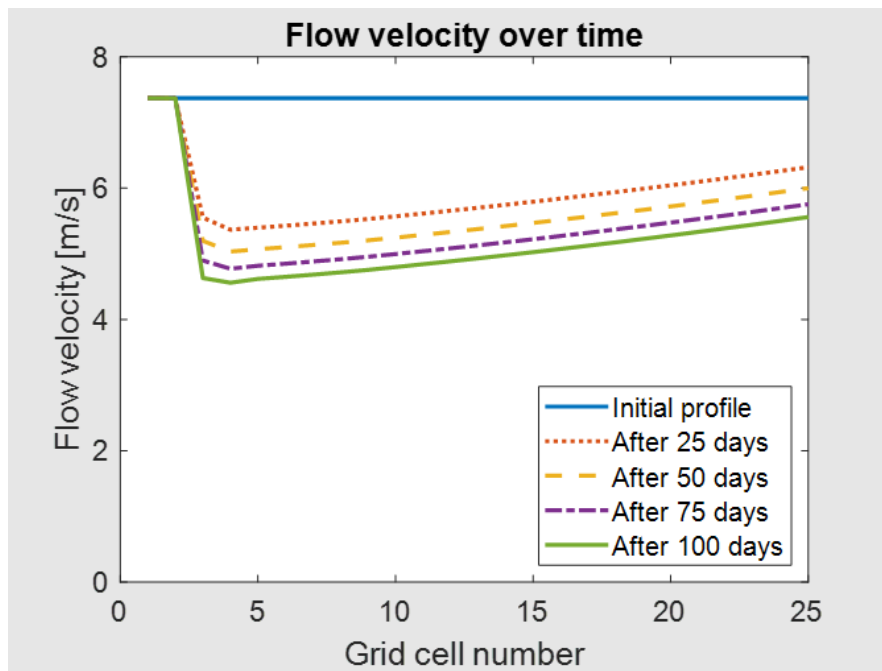


Figure 21. Flow velocity over time

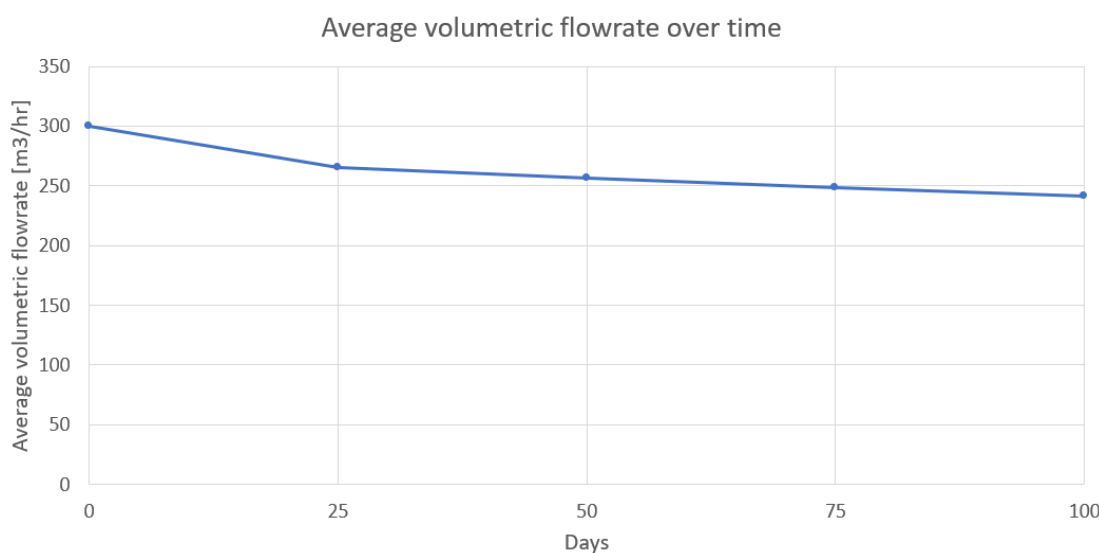


Figure 22. Average volumetric flowrate over time

The figures show a relative large reduction in flowrate after the first timestep, a reduction of 12.6 percent compared to the maximum flowrate without precipitation. This is due to the sudden change in surface roughness, as precipitation in the grid cells was not present beforehand. (Ceylan & Gudret, 2003) concluded that heat exchanger pipes have a surface roughness of 0.12 mm, which corresponds to a Fanning friction factor of 0.0053 in the modelled heat exchanger. After 25 days, precipitation has attached to the pipe walls, resulting in grid cell surface roughnesses ranging from 0.12 mm (where no precipitation occurred) to 0.34 mm, which corresponds to a Fanning friction factor of 0.0079. The flowrate decreases linearly in subsequent timesteps (a reduction of 3.1 percent after 50 days, compared to the flowrate after 25 days), as the deposition layer increases by roughly the same amount each timestep while roughness remains relatively constant. This means that the quality (location of precipitation) and quantity (precipitation amount per cell) of barite precipitation does not shift in the first 100 days.

5.3.3 Heat flux through pipe wall

The deposition of precipitated minerals also negatively affects the heat transfer in the heat exchanger, as the precipitation acts as an insulating layer. The impact of scaling on the exchange of heat can be categorized into two types:

- A change in heat convection from the brine to the precipitation layer, as the change in surface roughness and decrease in effective flow area impact the Nusselt number.
- An additional heat conduction layer due to the thickness of the deposition profile.

With increasing timesteps, the deposition layer grows larger, while the surface roughness is largely unaffected. Therefore, the change in radial heat transfer is much larger than the axial heat transfer variations (due to the precipitation peaks/crests). Thus, when analyzing the heat conduction, the deposition profile is modelled as an average thickness, instead of the inclusion of the peaks and crests. The average deposition thickness can also be written as a decrease in radius. This radial decrease, along with the thermal conductivity of barite, is used to calculate the conductive thermal resistance (Mills, 2014):

$$R_{\text{conductive,barite}} = \frac{\ln\left[\frac{r_{\text{I.D.}}+t}{r_{\text{I.D.}}}\right]}{2\pi * k_{\text{barite}} * L_{\text{cell}}}$$

Where:

- $R_{\text{conductive,barite}}$ is the conductive thermal resistance of the barite precipitation layer [K/W].
- $r_{\text{I.D.}}$ is the inner pipe radius [m].
- t is the average deposition layer thickness [m].
- k_{barite} is the thermal conductivity of barite [W/mK].

The peak and crests are, however, included in the calculation of the heat convection. The surface roughness profile impacts the flow profile close to the deposition and changes the heat transfer accordingly. Gnielinski's formula (Mills, 2014) links the flow profile and surface roughness to an averaged Nusselt number:

$$Nu_D = \frac{\frac{f}{8}(Re_D - 1000)Pr}{1 + 12.7\left(\frac{f}{8}\right)^{0.5}\left(Pr^{\frac{2}{3}} - 1\right)}$$

Where:

- Nu_D is the averaged Nusselt number for pipe flow [-].
- Pr is the Prandtl number [-].

The convective heat transfer coefficient is resolved from the Nusselt number (Mills, 2014).

$$h_{convective} = \frac{k_{barite}}{2 * (R_{pipe} - t_{precip.layer})} * Nu_D$$

From this parameter, the convective thermal resistance can be calculated:

$$R_{convective} = \frac{1}{2\pi * (R_{pipe} - t_{precip.layer}) * h_{convective} * L_{cell}}$$

Figure 23 provides the thermal resistance of conductive and convective heat transfer, respectively. Both resistances have the same order of magnitude at locations where no precipitation has occurred, but thermal resistance due to conduction becomes several times larger with respect to the thermal resistance of convection when precipitation is present. After the first timestep the conductive thermal resistance is 6 times larger at the location of minimal precipitation, and this difference grows linearly in time. Therefore the impact of scaling on convective heat transfer can be largely ignored within the time horizon of this simulation, and going forward the conductive heat transfer is the sole parameter which is varied to predict the heat transfer reduction over time.

The conductive heat transfer resistance is a combination of the thermal resistance of the stainless-steel pipe wall, which is constant over time, and the precipitation layer resistance, which increases over time:

$$R_{cond,total} = R_{cond,barite} + R_{cond,steel} = \frac{\ln\left[\frac{r_{I.D.}}{r_{I.D.-t}}\right]}{2\pi * k_{barite} * L_{cell}} + \frac{\ln\left[\frac{r_{O.D.}}{r_{I.D.}}\right]}{2\pi * k_{steel} * L_{cell}}$$

Where:

- $r_{O.D.}$ is the outer radius of the pipe [m].

Therefore, the heat transfer from the brine to the secondary flow decreases over time. This is visualized in Figure 24.

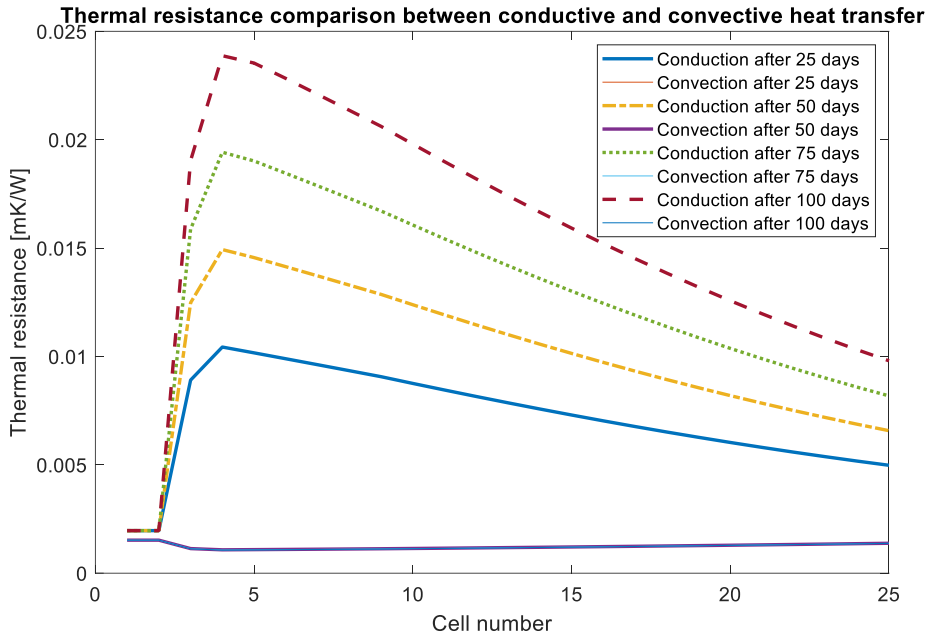


Figure 23: Thermal resistance comparison between conductive and convective heat transfer.

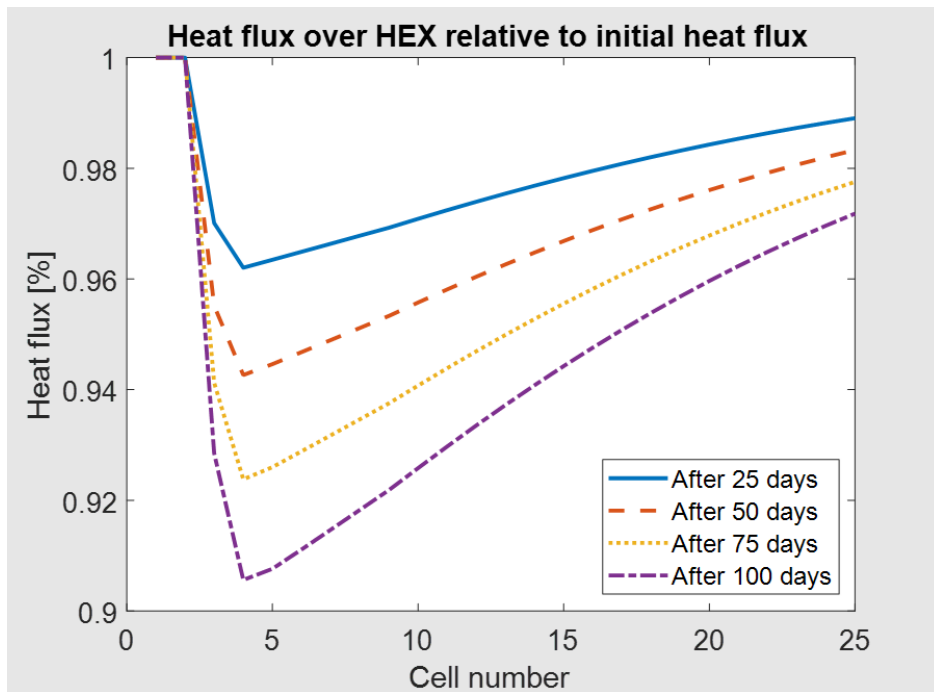


Figure 24: Relative changes in heat flux in heat exchanger (relative to the initial heat flux without any precipitation)

The heat flux in the heat exchanger is at a minimum at a location where the volumetric deposition reaches a maximum (cell 4), as the conductive thermal resistance scales with the volumetric deposition and is therefore also at a maximum. Further downstream in the heat exchanger, less barite precipitates, resulting in lower thermal resistances and thus a larger heat

flux compared to the initial cells. The drop in heat flux in the first 25 days is relatively large due to the initial formation of deposition, which has the largest impact on the hydrodynamics of the flow. Figure 25 shows that the average heat flux over the heat exchanger declines with roughly 2% of its original flux after a time period of 25 days. From 25 days onwards, the heat transfer reduces with roughly 1% every 25 days. When considering larger time scales, this decline will increase faster as the thermal resistance of the precipitation layer increases faster when smaller pipe diameters are concerned.

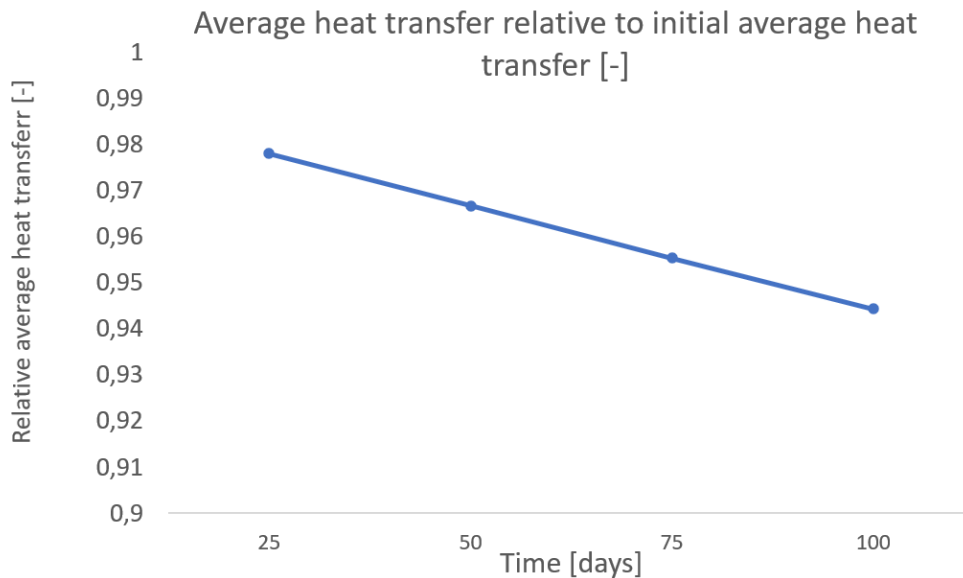


Figure 25: Relative average heat transfer in heat exchanger.

The reduction in heat transfer leads to higher brine temperatures in and after the heat exchanger, since less heat is dissipated. As a result, the temperature conditions of the cells change, which impacts mineral precipitation in the following timestep, which is not linear in time. Figure 26 shows the difference in precipitation volume at each cell after 100 days.

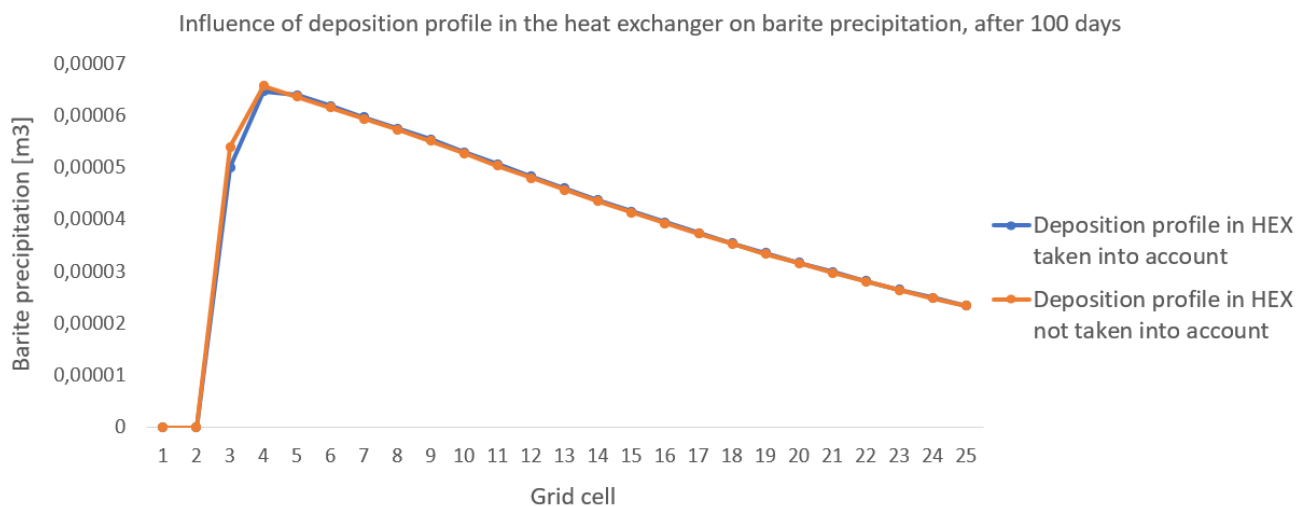


Figure 26: Influence of deposition profile in heat exchanger on barite precipitation

The temperature of the brine reduces less when a precipitation layer is present, resulting in relative higher brine temperatures in the heat exchanger. The solubility of barite is temperature driven, and its precipitation therefore shifts to the right: less barite precipitates in earlier cells, but this difference diminishes in the cells afterwards. The location of maximum precipitation will shift more downstream as larger time intervals are analyzed (e.g. a time interval of 200 days instead of 100 days), resulting in nonlinear differences between timesteps.

5.4 RESULTS CASE D: IMPACT OF UNCERTAINTIES ON SCALING

Minor variations in the composition of the brine lead to variations in the precipitation and deposition of critical minerals. An analysis is performed to determine the magnitude of these output variations. For this analysis, the nominal and percentual deviations of table 2 were used as input, and 100 samples were generated.

5.4.1 Uncertainty in deposition layer height

Each sample served as input for the precipitation model, returning the resulting deposition profile and volumetric flowrate per cell. The uncertainty in the deposition height of barite at each cell is shown in Figure 27.

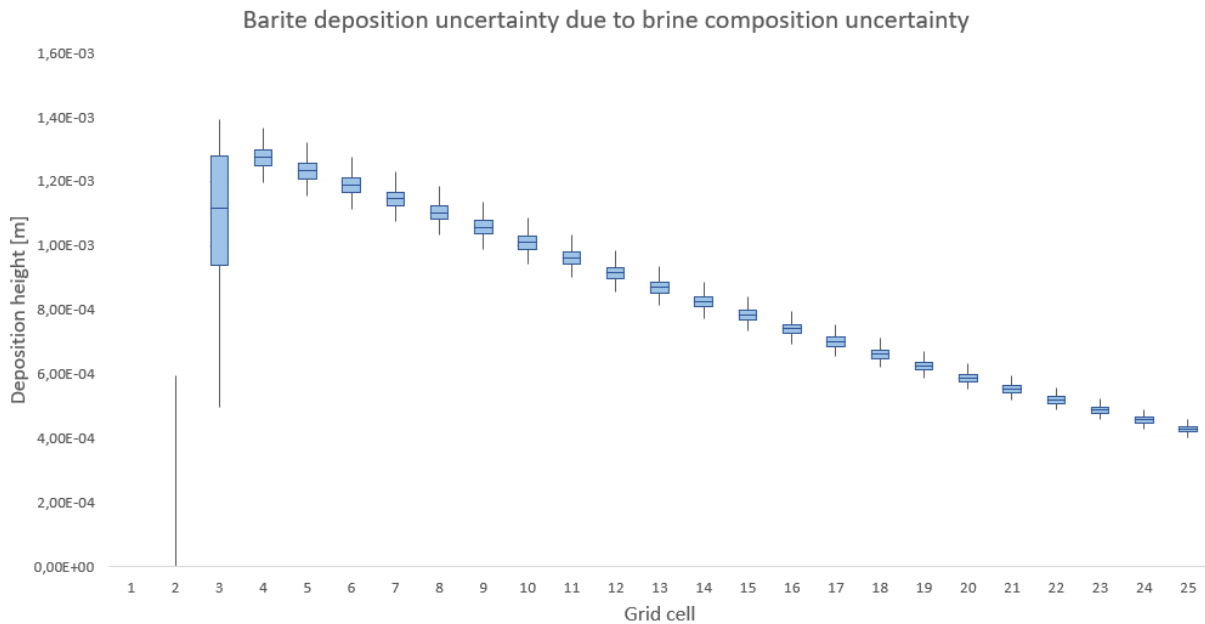


Figure 27. Deposition height uncertainty of barite precipitation

Large differences are present in the first number of cells, with the uncertainty boundaries converging as the cell number is increasing. The large uncertainties in cells 2 and 3 are a result of the saturation index being close to 1 for those specific cells due to the temperature in those cells being close to the temperature at which barite starts precipitating out of solution. No precipitation was present in cell 2 for the majority of the samples, and a small shift in mineral concentration give a relative large uncertainty when considering geothermal brine with a saturation ratio close to unity. The deviation from the median of cell 2 is around 25%. Further

downstream in the heat exchanger, at lower temperatures and lower solubility products of barite, the deviations become around 7%.

5.4.2 Uncertainty in flowrates

The uncertainty in barite precipitation also results in an averaged flowrate uncertainty. This is shown in Figure 28.

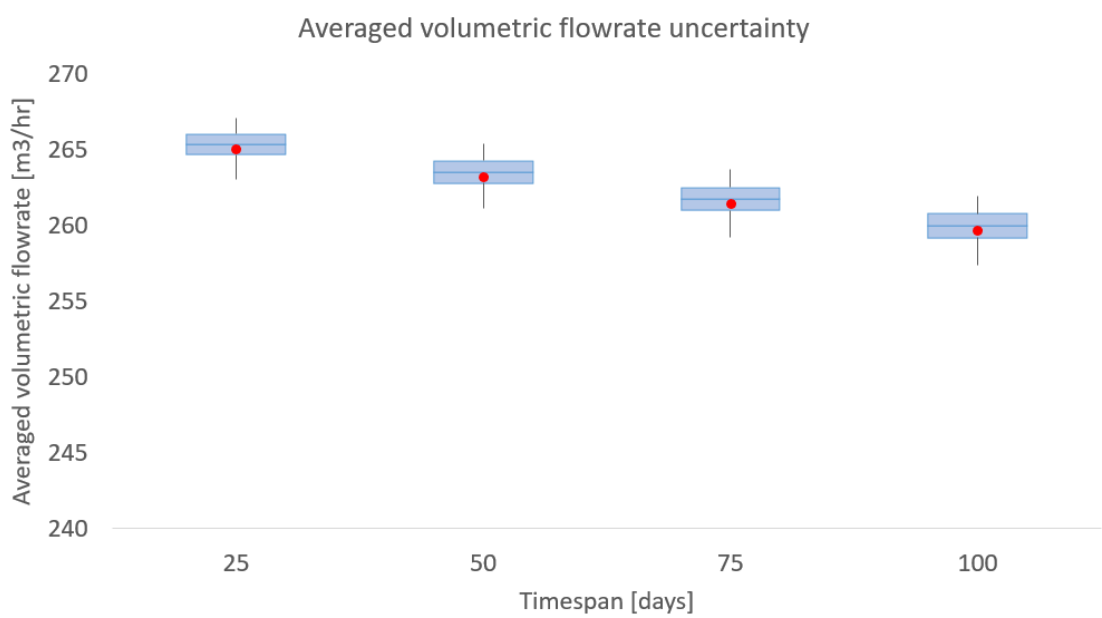


Figure 28. Uncertainty in averaged volumetric flowrate

The volumetric flowrate calculated with the nominal concentrations is roughly linearly decreasing in time. Slightly less barite will precipitate at later timesteps, as the brine temperature increases slightly over time due to the reduction in heat transfer, preventing some barite from precipitation. The red dot shows the averaged volumetric flowrate for the nominal case. Compared to the average of the 100 samples it is 0.2 m³/hr lower for each timestep. The uncertainty has an upper and lower boundary of 1% compared to the average, and it increases slightly for larger timesteps. Thus, an aleatoric uncertainty of 3-4% in the brine concentration leads to an average flowrate uncertainty of around 1%.

6 CONCLUSION & RECOMMENDATIONS

Within this task, a two-way coupled modelling approach was developed for the prediction of scaling, primarily barite, within geothermal systems. The approach uses a hydrodynamic flow solver (Drift-Flux) to calculate the flowrates, pressures, and temperatures in the system, and a geochemical speciation model (PHREEQC) to estimate the precipitation amounts of selected minerals at those conditions. Through newly developed deposition, roughness, and heat transfer models, the effects of precipitation are coupled back to changes in the flow, pressures, and temperatures in the system, which in turn lead to changes in precipitation amounts/locations.

In addition, to evaluate the effects of uncertainties in the measured composition of the geothermal brine, an uncertainty quantification workflow was developed and implemented, which generated a large number of possible brine compositions for which the scaling amounts would be calculated, allowing for analysis of the variation in predicted scaling amounts based on potential differences in brine composition.

Using the above two workflows in tandem, it is possible to use the models to predict occurrence and severity of various scaling types within a geothermal system, its effects on the decrease in flowrate over time, and the expected potential variation of these results based on the uncertainty in brine composition. In the next two sections, the main conclusions of current work and recommendations for future work are given.

6.1 CONCLUSIONS

6.1.1 Scaling model

A model was developed using the geochemical speciation software PHREEQC (Parkhurst & Appelo, 2013) to estimate the amount of barite precipitation with cooling. Two types of models were used to assess the maximum amount of scaling versus the time dependent precipitation. If the system would allow an equilibrium to be reached between barite and the fluid, an amount of $3.3E^{-5}$ mol/kgw barite is predicted to precipitate. When the reaction rate of barite using a 'kinetic' model is included, the amount of barite scaling is reduced several orders of magnitude to $7.70E^{-10}$ mol/kgw (for ten minutes of precipitation). These results indicate that caution is advised when assessing the barite precipitation simulations without reaction rates, as will be initially done for the workflow development. There are several factors besides the temperature affecting barite scaling, which have been investigated with the PHREEQC model. There is a strong kinetic control with the reaction rates of barite causing precipitation to be slow, requiring several years before equilibrium is reached at the new low temperature. Taking the reaction rates or a minimum required oversaturation (SI) for precipitation into account in geochemical modeling, considerably reduces the predicted barite scaling potential.

Besides the control of temperature, barite precipitation may also depend on the concentration of cations other than the main constituents. Incorporation of strontium forming a barite–celestite solid solution appears to reduce the total amount of scaling. The presence of increased

concentrations of calcium considerably reduces barite scaling as more cooling is required before barite starts coming out of the solution.

6.1.2 Impact of uncertainties on scaling

An uncertainty quantification analysis was performed on the effects of brine composition and ions concentration on the scaling potential and precipitation amount. In total eight elements were included in the analysis (barium, carbon, calcium, chlorine, potassium, magnesium, sodium, and sulphur), and 10,000 samples with different concentrations for each of these elements were generated. For each sampled brine composition the barite precipitation amount was calculated at five different temperature-pressure combinations.

Looking at the distribution of barite formation amounts, it was found that for higher temperatures, there were a significant amount of compositions for which no precipitation occurred at all. At a slightly higher temperature compared to the base case the precipitation can occur considering the brine composition uncertainties. In addition, it was found that uncertainties in barium, sulphur, calcium, and chlorine have the biggest impact on the amount of barite formed (i.e. changing the concentration of these elements results in a significant change to the amount of barite formed, while for the others it remains practically unchanged). Based on these results, any subsequent uncertainty quantifications performed on barite precipitation only focused on these four elements.

6.1.3 Impact of hydrodynamics on scaling

The deposition of barite was modelled as rows of cones, based on theory found in literature which describe mineral nucleation under geothermal conditions. A force balance was constructed which calculates the height at which the cones are sheared of due to hydrodynamic forces, resulting in trapezoidal structures. This structure was converted into a friction factor and a deposition thickness, which impact flow velocities, volumetric flowrates and heat transfer. The same modelling workflow was used to calculate the changes in the pressure for a given flow rate. Modelling of the brine composition given in Chapter 5 resulted in a relatively large reduction of flowrate in the first timestep (12.6 percent), which is due to the sudden change in surface roughness resulting from the initial precipitation. After the first timestep, the deposition layer grows radially inward in thickness, but the surface roughness does not change much. From the first timestep onward, a reduction of 3.1 percent in flowrate is observed every 25 days.

The impact of precipitation on the heat transfer was also modelled. Mineral precipitation results in a deposition layer on the pipe wall, which acts as an insulating layer, reducing heat transfer. The magnitude of the conductive thermal resistance outweighs the magnitude of the convective thermal resistance. The heat transfer reduces with 2 percent after 25 days, and with 1 percent after every 25 days, up to 100 days. The reduction in the initial 25 days is relatively large because flow hydrodynamics are affected more, due to initial precipitation.

Aleatoric uncertainty quantification is also performed to quantify the impact of composition uncertainties on the deposition layers. The largest variations in output were found in the first few cells, as the saturation index is close to 1 in these cells: some samples give a nonzero

expected precipitation, while others do not predict any precipitation. This leads to large uncertainties in earlier cells (around 25%) but to smaller uncertainties further downstream (around 7%). Converting these results in an averaged flowrate shows that the results deviate even less: the aleatoric uncertainty of 3-4% in the brine concentration leads to an average flowrate uncertainty of around 1%.

6.2 RECOMMENDATIONS

6.2.1 Scaling model

Current geochemical models were focused on barite, but other minerals can also precipitate alongside it. For example, celestite was shown to precipitate together with barite, but not yet included in the uncertainty analysis. Furthermore, a screening of other minerals predicted to be oversaturated in combination with measurements of scales from the pipes or precipitates in the filters of a geothermal plant would yield a more complete assessment of scaling in the geothermal system. Experimental work or a literature study on the saturation index required for barite scaling to commence would yield valuable data to make the assessment of barite scaling risks more accurate.

6.2.2 Impact of hydrodynamics on scaling

The uncertainties in strontium concentrations need to also be taken into account as it was shown that it can have a big impact on barite precipitation. The scaling prediction model was extended for kinetics to include the scaling reducing effect of slow reaction rates. However, the deposition model currently assumes that the entire amount of precipitate calculated per cell deposits within that same cell using the equilibrium PHREEQC model. Due to the kinetics of deposition, the location at which a solid mineral deposits on the wall is not necessarily the same location at which it first precipitates. Future work will also include kinetics in the deposition model to improve the estimation of the precise location and amounts of scaling deposits. Lastly, the validation and calibration of the models with experimental data is required to ensure the prediction accuracy.

6.2.3 Impact of uncertainties on scaling

Due to time constraints the number of samples included for the uncertainty quantification of the full two-way coupled modelling approach was limited to 100. To get more robust results, in the continuation of the activities this number will be increased. In addition, it could also be interesting to look at sampling from larger variations (current results focused only on the smaller well variations). Moreover, when modelling celestite or other materials, additional elements might have to be taken into account during the analysis (e.g. strontium for celestite modelling).

7 REFERENCES

- Abyzov, A. & Schmelzer, J., 2014. *Heterogeneous nucleation in solutions: Generalized Gibbs' approach*, Kharkov: AIP Publishing.
- Andritsos, N., Koutsoukos, P. & Karabelas, A., 2002. *Scale formation in geothermal plants*, Thessaloniki: Division of Earth Sciences.
- Anon., 2021. *calsep.com*. [Online]
Available at: <https://www.calsep.com/pvtsim-nova/>
- Azaza, H. et al., 2017. Calcite and barite precipitation in CaCO₃-BaSO₄-NaCl and BaSO₄-NaCl-CaCl₂ aqueous systems: kinetic and microstructural study. *Arabian Journal of Geosciences*, 10(10), pp. 1-9.
- Blount, C. W., 1977. Barite solubilities and thermodynamic quantities up to 300 degrees C and 1400 bars. *American Mineralogist*, 62(9-10), pp. 942-957.
- Boersma, A., Fischer, H. R. & Vercauteren, F., 2018. *Scaling assessment, inhibition and monitoring of geothermal wells*. Statford, 43rd Workshop on Geothermal Reservoir Engineering.
- Bouزيد, L., Belhadi, S., Yallese, M. A. & Mabrouki, T., 2014. *RMS-based optimization of surface roughness when turning AISI 420 stainless steel*, Guelma: International journal of materials and product technology.
- Ceylan, K. & Gudret, K., 2003. *The roughness effects of friction and heat transfer in the fully developed turbulent flow in pipes*, Baku: Applied Thermal Engineering.
- Chen, Z. et al., 2017. *Effect of modified starch on separation of fluorite from barite using sodium oleate*, Wroclaw: Physicochemical Problems of Mineral Processing.
- Dai, C. et al., 2021. *Prediction models of barite crystallization and inhibition kinetics: applications for oil and gas industry*, Houston: MDPI.
- Dai, Z., Kan, A., Zhang, F. & Tomson, M., 2014. A Thermodynamic Model for the Solubility Prediction of Barite, Calcite, Gypsum, and Anhydrite, and the Association Constant Estimation of CaSO₄(0) Ion Pair up to 250 °C and 22000 psi. *Journal of Chemical & Engineering Data*, 60(3), pp. 766-774.
- Haaland, S., 1983. *Simple and explicit formulas for the friction factor in turbulent pipe flow*, Copenhagen: Journal of Fluids Engineering.
- Haas-Nüesch, R. et al., 2018. *Mineralogical characterization of scalings formed in geothermal sites in the Upper Rhine Graben before and after the application of sulfate inhibitors*, Karlsruhe: Geothermics.
- Hammer, O., Lauritzen, S. E. & Jamtveit, B., 2011. *Stability of dissolution flutes under turbulent flow*, Bergen: Journal of Cave and Karts Studies.
- Heberling, M., 2017. *Genomics-based discovery and engineering of biocatalysts for conversion of animes*, Groningen: University of Groningen.
- Herman, J. & Usher, W., 2017. SALib: An open-source Python library for sensitivity analysis. *Journal of Open Source Software*, 2(9).
- Jones, F. et al., 2004. The effect of calcium ions on the precipitation of barium sulphate 1: calcium ions in the absence of organic additives. *Journal of Crystal Growth*, 262(1), pp. 572-580.
- Kristensen, L. et al., 2020. *PERFORM WP1: Learn and Understand (D1.3)*, s.l.: Geothermica.
- Lasaga, A. C. et al., 1994. Chemical weathering rate laws and global geochemical cycles. *Geochimica et Cosmochimica Acta*, 58(10), pp. 2361-2386.
- Lei, Q. et al., 2020. *Predicting activity coefficients with the Debye-Hückel theory using concentration dependent static permittivity*, Beijing: American Institute of Chemical Engineers.

- Mills, A., 2014. *Basic Heat and Mass Transfer*. Harlow: Pearson.
- Mirmanto, M., 2013. *Developing flow pressure drop and friction factor of water in copper microchannels*, Mataram: Journal of Mechanics Engineering and Automation.
- Monnin, C. & Cividini, D., 2006. *A thermodynamics and mineralogical study of the (Ba, Sr)SO₄ solid solution: Application to the calculation of the saturation state of the world's ocean with respect to the substituted barites*, Toulouse: Geochimica et Cosmochimica Acta.
- Osiptsov, A., Sin'kov, K. & Spesivtsev, P., 2014. *Justification of the Drift-Flux model for two-phase flow in a circular pipe*, Moscow: Pleiades Publishing Ltd..
- Palandri, J. L. & Kharaka, Y. K., 2004. *A compilation of rate parameters of water-mineral interaction kinetics for application to geochemical modeling*, Menlo Park, California: U.S. Geological Survey.
- Parkhurst, D. & Appelo, C., 2013. Description of input and examples for PHREEQC version 3 - A computer program for speciation, batch-reaction, one-dimensional transport, and inverse geochemical calculations. *U.S. Geological Survey Techniques and Methods*.
- Regenspurg, S. et al., 2014. *Mineral precipitation during production of geothermal fluid from a Permian Rotliegendes reservoir*, Potsdam: Geothermics.
- Saltelli, A. et al., 2010. Variance based sensitivity analysis of model output. Design and estimator for the total sensitivity index. *Computer Physics Communications*, pp. 259-270.
- Schreiber, S., Lapanje, A., Ramsak, P. & Breembroek, G., 2016. *Operational Issues in Geothermal Energy in Europe - Status and Overview*, Reykjavik: Coordination Office, Geothermal ERA NET.
- Schutte, K., 2016. *A hydrodynamic perspective on the formation of asphaltene deposits*, Delft ISAPP Integrated systems approach to petroleum production.
- Sorbie, K. & Scott Boak, L., 2012. *The effects of barium sulfate saturation ratio, calcium, and magnesium on the inhibition efficiency - part 1: Phosphonate scale inhibitors*, Edinburgh: SPE Productions & Operations.
- Tranter, M., De Lucia, M., Wolfgramm, M. & Kuhn, M., 2020. *Barite scale formation and injectivity loss models for geothermal systems*, Potsdam: MDPI.
- Twerda, A. & Veltin, J., 2014. *Building blocks of asphaltene modelling: A combination of sub-models to quickly assess mitigation strategies*. s.l., s.n.
- van der Hulst, T., 2019. *Injectivity reduction in geothermal wells*, Delft, the Netherlands: Petroleum Engineering and Geo-sciences.
- Wang, H. et al., 2013. *Formation of CaCO₃ deposits on hard surfaces - effect of bulk solution condition and surface properties*, Ludwigshafen: Applied materials & interfaces.
- Wasch, L., Shoeibi-Omrani, P. & Twerda, A., 2019. *Integrated Scale Management for Geothermal*. s.l., s.n.
- Wen, C. et al., 2020. *Experimental research and sensitivity analysis of mudstone similar materials based on orthogonal design*, Hindawi: Materials Science and Engineering.
- Wright, M. R., 2007. *An introduction to aqueous electrolyte solutions*. Chichester: John Wiley & Sons, Ltd.
- Yan, F. et al., 2016. *Scale formation and control under turbulent conditions*, Aberdeen: Society of Petroleum Engineers.
- Zhang, J., 2020. Modern Monte Carlo Methods for Efficient Uncertainty Quantification and Propagation. *Wiley Interdisciplinary Reviews: Computational Statistics*, Volume 13.

Zhen Wu, B. Y., 2016. *A Combined Thermodynamic and Kinetic Model for Barite Prediction at Oil Reservoir Conditions*, s.l.: Department of Chemistry, Faculty of Science, University of Copenhagen.